A CUSTOM DESIGN TEMPERATURE-CONTROLLED LASER SYSTEM FOR MEDICAL APPLICATIONS

by

Batuhan Dizman

B.S. in Electrical-Electronics Engineering, Işık University, 2010

Submitted to the Institute of Biomedical Engineering
in partial fulfillment of the requirements
for the degree of
Master of Science
in
Biomedical Engineering

Boğaziçi University
2024

A CUSTOM DESIGN TEMPERATURE-CONTROLLED LASER SYSTEM FOR MEDICAL APPLICATIONS

APPROVED BY:

Assist. Prof. Dr Mustafa Kemal Ruhi .....
(Thesis Advisor)

Assoc. Prof. Dr. Onur Ferhanoğlu .....

Prof. Dr. Ahmet Ademoğlu .....

DATE OF APPROVAL: 12 June 2024

ACKNOWLEDGMENTS

I would like to thank my supervisor, Assist. Prof. Dr. Mustafa Kemal Ruhi, for his sincere guidance and contributions to my thesis. I am also grateful to Prof. Dr. Murat Gülsoy for helping me selecting the thesis topic.

I would like to thank to my friend and colleague, Satuk Buğra Tekin, for his utmost contributions in compiling the software library of the system.

I would like to express my gratitude to Assoc. Prof. Dr. Onur Ferhanoğlu and Prof. Dr. Ahmet Ademoğlu for being a member of my thesis committee.

I am deeply grateful to my wonderful wife, Elif, for encouraging me to return to the institute and for her unwavering emotional support throughout my master's thesis journey.

I am endlessly thankful to my dear mother and sister for their unshakable support since 2010, the very start of my journey toward earning my master's degree.

ACADEMIC ETHICS AND INTEGRITY STATEMENT

I, Batuhan Dizman, hereby certify that I am aware of the Academic Ethics and Integrity Policy issued by the Council of Higher Education (YÖK) and I fully acknowledge all the consequences due to its violation by plagiarism or any other way.

Name :

Signature:

Date:

ABSTRACT

A CUSTOM DESIGN TEMPERATURE-CONTROLLED LASER SYSTEM FOR MEDICAL APPLICATIONS

Photothermal treatments are researched in multiple medical applications, including the treatment of vascular lesions and malignant tumors, as well as laser resurfacing and laser tissue welding. Optimal laser energy delivery to target tissue is important to achieve an effective treatment with minimal damage to healthy tissue. However, this can be challenging because optical properties may vary depending on tissue type and environmental factors. Therefore, real-time measurement of temperature is as important as dosimetry for a successful and safe photothermal laser applications. In addition, the temperature measurement must be non-contact to minimize the risk of microbial contamination. In this study, we developed a temperature-controlled 808 nm diode-laser system that eliminates the risk of thermal damage and contamination by performing non-contact, real-time temperature measurements of the irradiated surface. The system is composed of an 808 nm c-mount diode laser, an infrared (IR) array sensor for temperature measurement, a PC, and an electronic control unit (ECU). The system was tested on phantoms and *ex vivo*. tissues. According to the results, the temperature-controlled 808 nm diode-laser system could maintain the surface temperature of samples at the target temperature value.

Keywords: Photothermal laser applications, Temperature-controlled laser systems, Infrared array sensors.

ÖZET

TIBBİ UYGULAMALARA YÖNELİK ÖZEL TASARIM SICAKLIK KONTROLLÜ LAZER SİSTEMİ

Fototermal terapi, vasküler lezyonlar ve kötü huylu tümörlerin hem de doku birleştirme ve yenileme tedavileri de dahil olmak üzere çeşitli tıbbi uygulamalarda araştırılmakta olan bir tedavi tekniğidir. Sağlıklı dokuda oluşabilecek minimum zararla etkili bir tedavi elde etmek için, hedef dokuya optimal lazer enerjisi uygulamak önemlidir. Ancak optik özellikler doku tipine ve çevresel faktörlere bağlı olarak değişebileceği için işlemi zorlaştırabilir. Bu nedenle, başarılı ve güvenli fototermal lazer uygulamaları için dozimetri kadar gerçek zamanlı sıcaklık ölçümü de önemlidir. Ek olarak, sıcaklık ölçümünün mikrobiyal kontaminasyon riskini en aza indirmek için ölçüm esnasında temas olmaması gerekir. Bu çalışmada, ısıl hasar ve kontaminasyon riskini ortadan kaldıran, ışınlanan yüzeyin temas etmeden gerçek zamanlı sıcaklık ölçümlerini alabilen, sıcaklık kontrollü 808 nm diyot lazer sistemini geliştirdik. Sistem, 808 nm c-mount diyot lazer, sıcaklık ölçümü için kızılötesi (IR) dizi sensörü, bilgisayar ve elektronik kontrol ünitesinden oluşmaktadır. Sistem, fantomlar ve labaratuvar ortamındaki dokularda test edilmiştir. Sonuçlara göre, sıcaklık kontrollü 808 nm diyot lazer sistemi, örneklerin yüzey sıcaklığını hedef sıcaklığı değerinde tutabilmiştir.

Anahtar Sözcükler: Fototermal lazer uygulamaları, Sıcaklık kontrollü lazer sistemi, İnfrared dizi sensörleri

TABLE OF CONTENTS

ACKNOWLEDGMENTS . . . iii
ACADEMIC ETHICS AND INTEGRITY STATEMENT . . . iv
ABSTRACT . . . v
ÖZET . . . vi
LIST OF FIGURES . . . ix
LIST OF TABLES . . . xii
LIST OF SYMBOLS . . . xiii
LIST OF ABBREVIATIONS . . . xiv
1. INTRODUCTION . . . 1
1.1 Aim of the Study . . . 2
2. MATERIALS: DESIGN OF TEMPERATURE-CONTROLLED LASER SYSTEM . . . 4
2.1 Power Unit . . . 5
2.2 Electronic Control Unit (ECU) . . . 6
2.2.1 Design Considerations . . . 7
2.2.2 Current Sense and Voltage Monitoring Circuit . . . 8
2.2.3 Current Control Circuit . . . 9
2.2.4 Power OP-AMP . . . 11
2.2.5 Power Supply . . . 12
2.2.6 Microcontroller Unit . . . 13
2.2.7 Communication Interfaces . . . 14
2.2.8 PT-500 Temperature Measurement Circuit . . . 15
2.2.9 Other Peripherals . . . 16
2.2.10 Electronic Control Unit PCB Design . . . 16
2.3 IR Array Unit . . . 18
2.3.1 Design Considerations . . . 20
2.3.2 IR Array Module Design . . . 21
2.3.3 IR Array Unit PCB Design . . . 22
2.4 Installation of The System . . . 24

2.5 User Interface 25
2.6 Power vs Laser Diode Current 26
3. METHODS 28
3.1 Temperature Measurement Using the IR Array Sensor and Comparison with a Commercial IR Thermometer 28
3.2 Temperature-Controlled Laser System Flowchart 29
3.3 Preliminary Studies 30
3.4 System Improvements 32
3.5 Photothermal Applications 34
4. RESULTS 36
4.1 Comparison of IR Array Sensor with a Commercial IR Thermometer . 36
4.2 Preliminary Studies 37
4.3 Photothermal Applications 38
4.4 Constant Power Irradiation of Lamb Liver Tissue 44
5. DISCUSSION 46
APPENDIX A. SCHEMATICS OF ELECTRONIC CONTROL UNIT 48
APPENDIX B. PCB DESIGN OF ELECTRONIC CONTROL UNIT 51
APPENDIX C. SCHEMATICS OF IR ARRAY UNIT 52
APPENDIX D. PCB DESIGN OF IR ARRAY UNIT 54
REFERENCES 55

LIST OF FIGURES

Figure 1.1	Photothermal effects of laser.	2
Figure 2.1	Temperature-controlled laser system.	4
Figure 2.2	Detailed images of power unit.	5
Figure 2.3	Block diagram of electronic control unit.	6
Figure 2.4	Simplified schematics of the laser control system.	7
Figure 2.5	Schematics of current sense circuit.	9
Figure 2.6	Schematics of current control circuit.	10
Figure 2.7	Schematics of power op-amp.	11
Figure 2.8	Schematics of the power supply of electronic control unit.	12
Figure 2.9	Schematics of PT-500 temperature measurement circuit.	15
Figure 2.10	Printed circuit board of electronic control unit.	17
Figure 2.11	The 650-nm 5mW positioning laser.	18
Figure 2.12	Block diagram of IR Array Unit.	19
Figure 2.13	The Heimann Sensor HTPA32x32dR2L5.0 pixels.	21
Figure 2.14	Schematics of The Heimann Sensor HTPA32x32dR2L5.0 module.	22
Figure 2.15	Design of the printed circuit board of IR array unit and the assembled PCB	23
Figure 2.16	Front and rear view of the system	24
Figure 2.17	User interface program.	26
Figure 2.18	Laser output power vs current.	27
Figure 3.1	Raytek Raynger ST IR thermometer.	28
Figure 3.2	(a) Laser control flowchart for agar gel irradiation. (b) Laser control flowchart for lamb liver irradiation.	29
Figure 3.3	Agar gel experiment setup.	30
Figure 3.4	Lamb liver experiment setup.	31
Figure 3.5	(a) Flowchart of temperature detection rate function. (b) Updated flowchart of laser irradiation control.	32
Figure 3.6	Temperature-controlled laser system setup.	33
Figure 3.7	FOV calculation according to viewing angle and target distance.	34

Figure 4.1 Comparison of IR array sensor with a commercial IR thermometer(C.T.). 36

Figure 4.2 Box and whisker plot of the temperatures after the samples reach the target temperature, 42.5°C, as indicated by the dashed line. 38

Figure 4.3 (a) Temperature of agar gel (left y-axis, indicated as blue) and laser current (right y-axis, indicated as red) during irradiation at a target temperature of 42.5°C.(b) Temperature of lamb liver tissue (left y-axis, indicated as green) and laser current (right y-axis, indicated as red) during irradiation at a target temperature of 42.5°C. 39

Figure 4.4 (a) Temperature of agar gel (left y-axis, indicated as blue) and laser current (right y-axis, indicated as red) during irradiation at a target temperature of 42.5°C. (b) A 32x32 heat map was acquired at an instant during agar gel irradiation at a target temperature of 42.5°C. (c) Temperature of lamb liver tissue (left y-axis, indicated as green) and laser current (right y-axis, indicated as red) during irradiation at a target temperature of 50°C. (d) A 32x32 heat map was acquired at an instant during the irradiation of lamb liver tissue at a target temperature of 50°C 40

Figure 4.5 (a) Temperature of lamb liver tissue (left y-axis, indicated as blue) and laser current (right y-axis, indicated as red) during irradiation at a target temperature of 60°C. (b) A 32x32 heat map was acquired at an instant during the irradiation of lamb liver tissue at a target temperature of 60°C. (c) Temperature of lamb liver tissue (left y-axis, indicated as green) and laser current (right y-axis, indicated as red) during irradiation at a target temperature of 70°C. (d) A 32x32 heat map was acquired at an instant during the irradiation of lamb liver tissue at a target temperature of 70°C 41

Figure 4.6 (a) Box and whisker plot of the temperatures agar gel reach the target temperature, 42.5°C, as indicated by the dashed line. (b) Box and whisker plot of the temperatures lamb liver reach the target temperature, 50°C, as indicated by the dashed line. (c) Box and whisker plot of the temperatures lamb liver reach the target temperature, 60°C, as indicated by the dashed line. (d) Box and whisker plot of the temperatures lamb liver reach the target temperature, 70°C, as indicated by the dashed line. 42

Figure 4.7 (a) Lamb liver tissue irradiated at 50°C (b)Lamb liver tissue irradiated at 60°C (c)Lamb liver tissue irradiated at 70°C 43

Figure 4.8 (a) Constant power irradiation of lamb liver tissue for 42.5°C. (b) Constant power irradiation of lamb liver tissue for 50°C (c) Constant power irradiation of lamb liver tissue for 60°C (d) Constant power irradiation of lamb liver tissue for 70°C 44

Figure A.1 Schematics design of electronic control unit sheet1. 48

Figure A.2 Schematics design of electronic control unit sheet2. 49

Figure A.3 Schematics design of electronic control unit sheet3. 50

Figure B.1 PCB design of ECU. 51

Figure C.1 Schematics design of IR array unit sheet1. 52

Figure C.2 Schematics design of IR array unit sheet2. 53

Figure D.1 PCB design of IR array unit. 54

LIST OF TABLES

Table 2.1 The factory default configuration of the HTPA32x32dR2L5.0 Heimann Sensor IR Array module. 20

Table 4.1 Measurement results of IR array sensor and commercial IR thermometer (C.T.) in terms of °C degree Celsius. 37

Table 4.2 The 25% and 75% percentiles for lamb liver tissues according to Figure 4.6b, Figure 4.6c and Figure 4.6d. 43

LIST OF SYMBOLS

A	Ampere
cm	Centimeter
$I_{LaserDiode}$	Laser Diode Current
Kbps	Kilobits per second
nm	Nanometer
MHz	Megahertz
mm	Millimeter
mW	MilliWatt
nF	Nanofarad
P	Power
pF	Picofarad
R	Resistor
s	Seconds
uA	Microampere
um	Micrometer
V	Voltage
VCC	Common Collector Voltage
V_F	Forward Voltage
V_{Ref}	Reference Voltage
W	Watt
Ω	Ohm
°C	Degree Celcius

LIST OF ABBREVIATIONS

ADC	Analog-to-Digital Converter
C.T.	Commercial Thermometer
CW	Continuous Wave
DAC	Digital-to-Analog Converter
ECU	Electronic Control Unit
FOV	Field-of-view
FPS	Frames per second
HASL	Hot Air Solder Leveling
IC	Integraetd Circuit
IR	Infrared
I2C	Inter-Integrated Circuit
JTAG	Joint Test Action Group
LASER	Light Amplification by Stimulated Emission of Radiation
LED	Light-Emitting Diode
LITT	Laser-Induced Thermal Therapy
LQPF	Low-Profile Quad Flat Package
MCU	Microcontroller Unit
OP-AMP	Operational Amplifier
PC	Personal Computer
PCB	Printed Circuit Board
PCTL	Percentile
QFN	Quad Flat No-Lead Package
SMPS	Switch Mode Power Supply
SPI	Serial Peripheral Interface
SWD	Serial Wire Debug
UART	Universal Asynchronous Receiver and Transmitter
USB	Universal Serial Bus

1. INTRODUCTION

Lasers are used in medical applications since the very beginning of its invention [1]. Laser tissue interaction mechanisms are categorized into photochemical interaction, photothermal interaction, plasma-induced ablation, photoablation and photodisturption. The energy density, exposure time and wavelength of the laser determines the type of the interaction [2].

The mechanism of photothermal interactions consist of the following steps: absorption of light, conversion of light to heat, heat dissipation and eventually photothermal effect. Tissue contains molecules such as water, hemoglobin, melanin, and other chromophores that can absorb light at specific wavelengths. When light penetrates tissue, these chromophores absorb photons, elevating their energy states. The molecules experience vibrational and rotational transitions, transforming the photon energy into heat. This results in a rise in temperature in the surrounding tissue. The rate of the heat dissipation is influenced by factors such as tissue composition, blood flow, and thermal conductivity [2].

Photothermal effects of the laser on the tissue, as seen in Figure 1.1, can be described as hyperthermia, coagulation, vaporization, carbonization and melting. Each of these biological effects occurs within a narrow range of temperatures where $>45°C$ for hyperthermia, $>50°C$ reduction of enzyme activity and cell immobility, $>60°C$ for coagulation, $>100°C$ vaporization and carbonization, $>300°C$ melting [2]. In order to achieve the desired treatment, the tissue must be maintained within the specified temperature range; otherwise, irreversible thermal damage will occur.

In photothermal treatments, temperature increase induced by laser irradiation is used for medical applications including laser resurfacing and the treatments of vascular lesions and malignant tumors [3–9]. Clinical application of photohermal therapies requires a precise temperature increase, which is challenging due to the varying optical

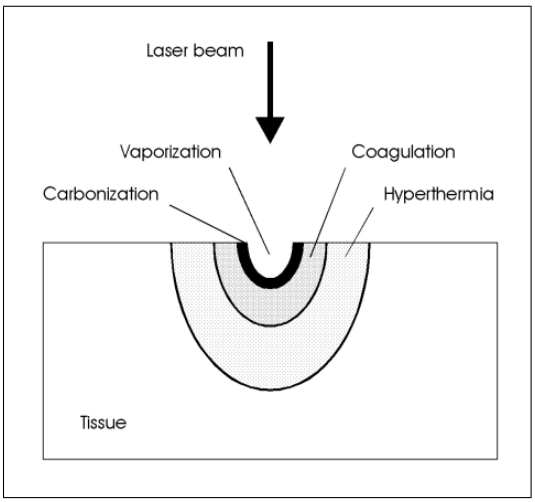


Figure 1.1 Photothermal effects of laser.

properties of different tissues [10]. Although dosimetry studies help determine optimal laser parameters for a specific tissue, tissue properties may also differ according to other factors, including ambient temperature, water amount in the tissue, and health condition of the patient [11]. Therefore, precise control of the tissue temperature in a photohermal therapy applications is crucial for achieving the expected treatment outcome, as well as avoiding damage to the surrounding tissue.

Real-time temperature measurement during laser irradiation and temperature-controlled laser systems were previously researched by multiple groups [12–16]. Although they are efficient and relatively cheap, thermocouples are not feasible due to the risk of contamination and the potential of interference with the measurement. IR-based temperature measurements, on the other hand, provide a fast and accurate temperature measurement with no risk of contamination, although they are relatively expensive and can only measure surface temperature.

1.1 Aim of the Study

In this study, we aimed to develop a temperature-controlled 808 nm diode-laser system and optimize this system for the irradiation of different samples. To achieve this goal, a 32x32 pixel IR array sensor and an 808 nm laser diode were purchased.

The rest of the hardware and software were developed from scratch. The array-based sensor enabled us to select the area where we wanted to acquire temperature data. According to the results, the system was able to measure the surface temperature of the phantom and liver tissue and adjust the laser output power accordingly. After further optimization and development, the proposed system can be used for effective and safe photothermal therapy applications in clinics.

2. MATERIALS: DESIGN OF TEMPERATURE-CONTROLLED LASER SYSTEM

Temperature-controlled laser system consists of power unit, electronic control unit(ECU), IR array unit and 808 nm diode laser. An 808 nm 5W cw C-Mount Laser diode (Zhuhai AIKE Photonics Technology Co., Ltd) was purchased and placed into an aluminum box. The laser is connected to electronic control unit (ECU), and its operation is controlled via voltage-controlled current. The required current and voltage is supplied through a power unit. The ECU is connected to a personal computer (PC) via USB and to the IR Array unit via RS-232. In addition IR array unit is also connected to a PC via RS-485. The whole setup was mounted on a platform made of sigma profile as shown in Figure 2.1.

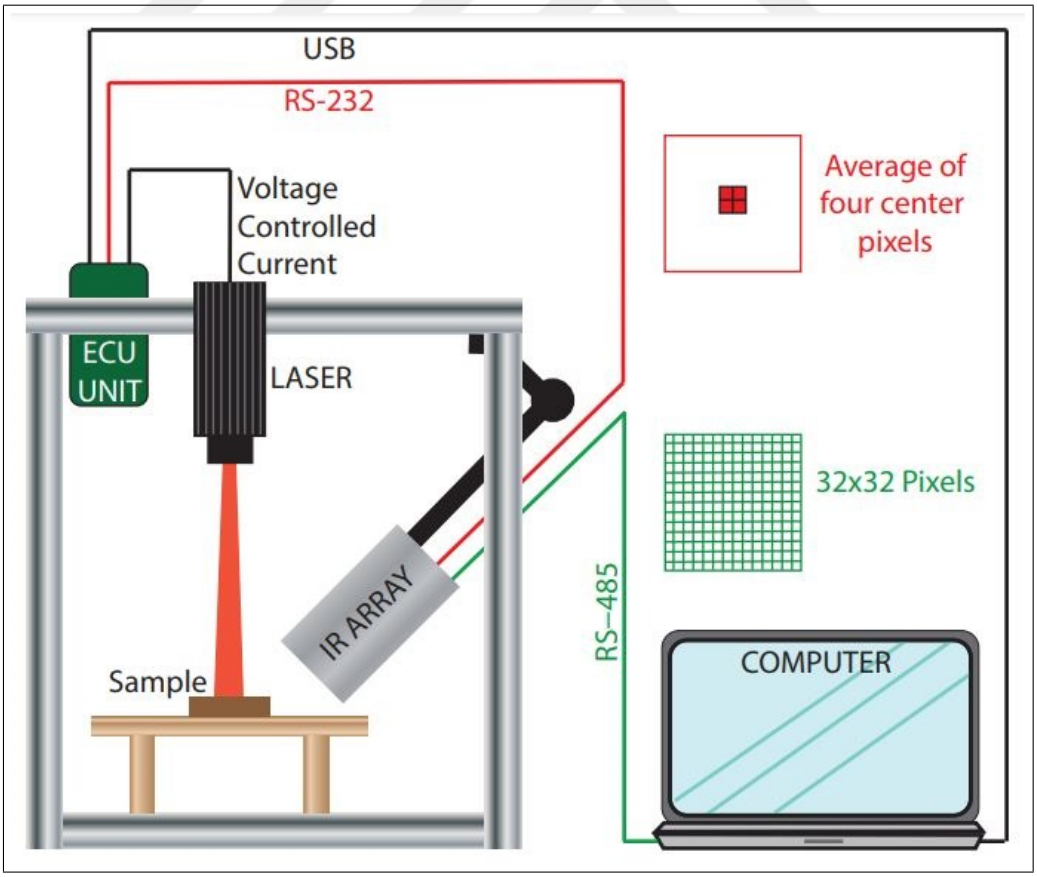


Figure 2.1 Temperature-controlled laser system.

In this setup, USB, RS-232, and RS-485 communication layers operate at a speed of 115 kbps. The ECU receives the average temperatures of the four center pixels from the target via the IR array unit using RS-232 communication. Meanwhile, a 32x32 pixel grid of target temperatures can be monitored via RS-485 from the PC. We have used Hercules in PC, a free serial port terminal software, to monitor and send commands via RS-485 or RS-232 terminals. The two printed circuit boards (PCB) that control and operate the system were designed from scratch. PCB design and schematics can be found in APPENDIX A, APPENDIX B, APPENDIX C and APPENDIX D.

2.1 Power Unit

The power unit of the system consists of fuse, SMPS unit, ON-OFF switch and the enclosure as shown in Figure 2.2. The SMPS unit of the system is EDR-120-12 which is manufactured by Mean Well and it provides 12V 10A output. It has universal input voltage range which is 90-264VAC. The SMPS unit has protection of over voltage, over temperature, overload and short circuit [17].



Figure 2.2 Detailed images of power unit.

While the SMPS unit provides the required current and voltage, the 10A DIN rail fuse provides additional electrical protection. The ON-OFF switch enables the user to easily turn the system on and off. When the LED inside the button lights up, it indicates that the system has turned on. The enclosure has been chosen as plastic, and the input and output cables are connected through cable glands to ensure electrical safety.

2.2 Electronic Control Unit (ECU)

The electronic control unit is primarily responsible for the operation of the system. The system simultaneously controls the output power of the laser diode while measuring both the current and voltage applied to the diode.

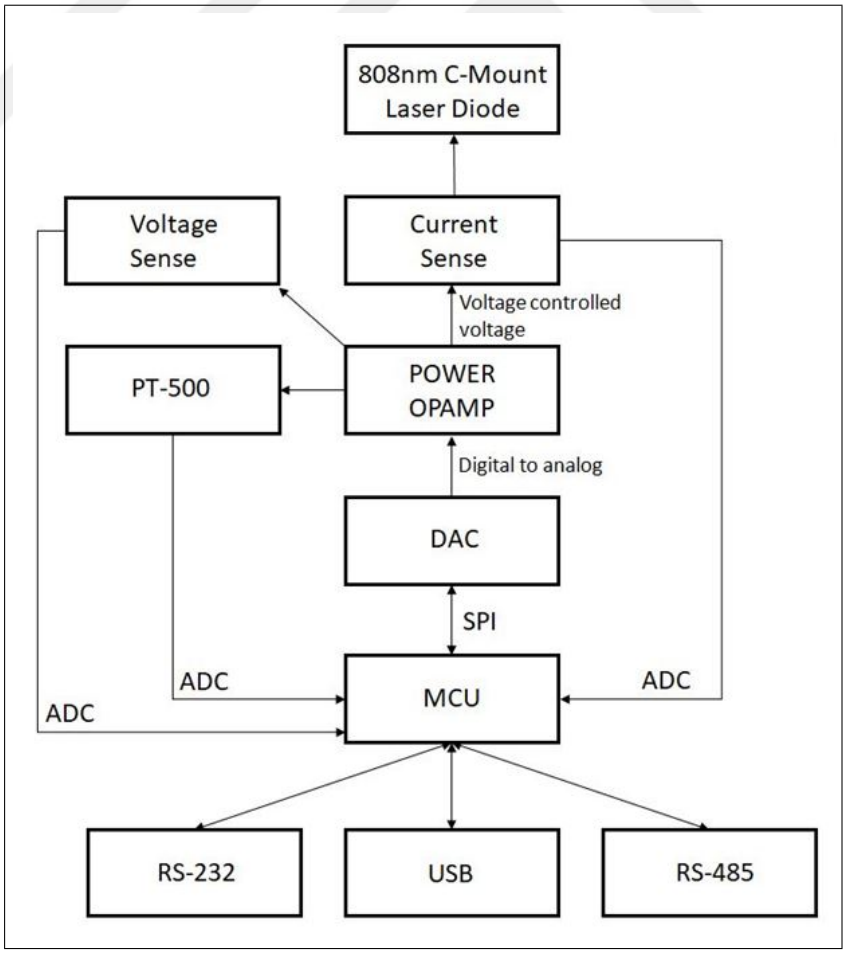


Figure 2.3 Block diagram of electronic control unit.

Additionally, the output voltage is regulated through the power operational amplifier, which is connected to the digital-to-analog converter (DAC). The DAC is controlled by the microcontroller unit (MCU) via SPI. The controlling process generates heat on the power operational amplifier (op-amp). Therefore, an aluminum heat sink is attached to the op-amp, and the temperature of the op-amp is also measured using a PT-500 sensor. Throughout the measuring process, the heat, current, and voltage are connected to the analog-to-digital converter (ADC) of the MCU.

The USB layer is connected to PC and RS-232 layer is connected to IR array unit. RS-485 communication layer of the system is reserved for future use. When the USB is connected to a computer, a COM port automatically opens in the operating system, so that any computer with free serial terminal software can use the system.

2.2.1 Design Considerations

The electronic components of the system were chosen according to the system requirements. The 5W cw laser diode requires 5A for maximum output power. Therefore the power op-amp was chosen as OPA549 which can supply 8A continuous and 10A peak current [18]. The simplified version of the controlling system can be seen in Figure 2.4, where the power resistor value remains same the VCC is regulated by power op-amp.

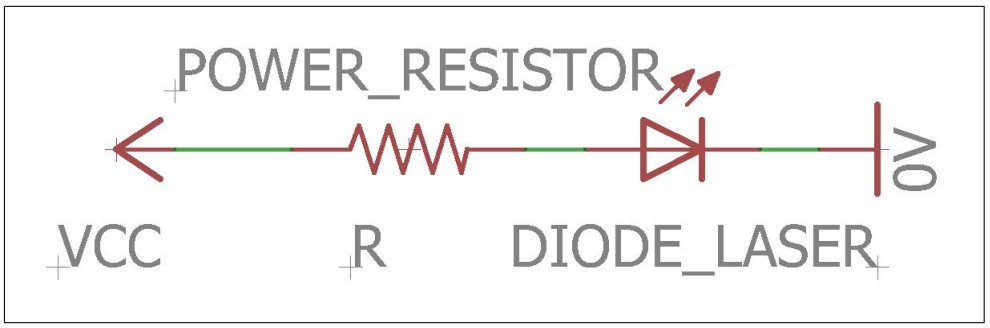


Figure 2.4 Simplified schematics of the laser control system.

While the resistance (R) and laser diode forward voltage (V_F) values remain constant, any changes in the VCC value result in a change in the current ($I_{LaserDiode}$)

flowing through the laser diode as seen in Eq. 2.1.

$$I_{LaserDiode} = \frac{VCC - V_F}{R} \tag{2.1}$$

The value of the resistor chosen is 1 Ω, and the maximum current flowing through the resistor is 5A. Therefore, the power dissipated by the resistor (R) can be calculated using the formula $P = I^2R$, which yields 25W. To ensure a safety margin and accommodate potential variations, a 50W 1 Ω aluminum case power resistor was selected. The resistor placed in an aluminum enclosure and mounted on sigma profile.

2.2.2 Current Sense and Voltage Monitoring Circuit

The current sense circuit of the ECU detects the current flow through the diode laser, and simultaneously, the measured current is monitored from the computer. LT6105CMS8#PBF current sense amplifier is selected. The current is calculated by the equation 2.2 where R83 equals to R84 and L3 is short circuit. In this case R83 and R84 chosen as 100Ω, and R108 and R109 chosen as 2.5kΩ, so the gain of the current sense circuit is calculated as 50 [19].

$$V_{CurrentSense} = (V_{Vout} - V_{VOUTCONT}) \cdot \frac{R108 + R109}{R83} \tag{2.2}$$

CURRENT_MONITORING node is connected directly to ADC of the MCU rather than connecting CURRENT_SENSE node to ensure electrical safety of the MCU. In the event of a short circuit of the diode laser, the maximum output voltage of the current sense circuit would equal the supply voltage of the amplifier. In the worst-case scenario, the 6.2V zener diode (D5) will clamp the output voltage to 6.2V.

This clamped output voltage will then be divided into two, resulting in a safe zone of 3.1V. The C64 on the other hand provides noise reduction.

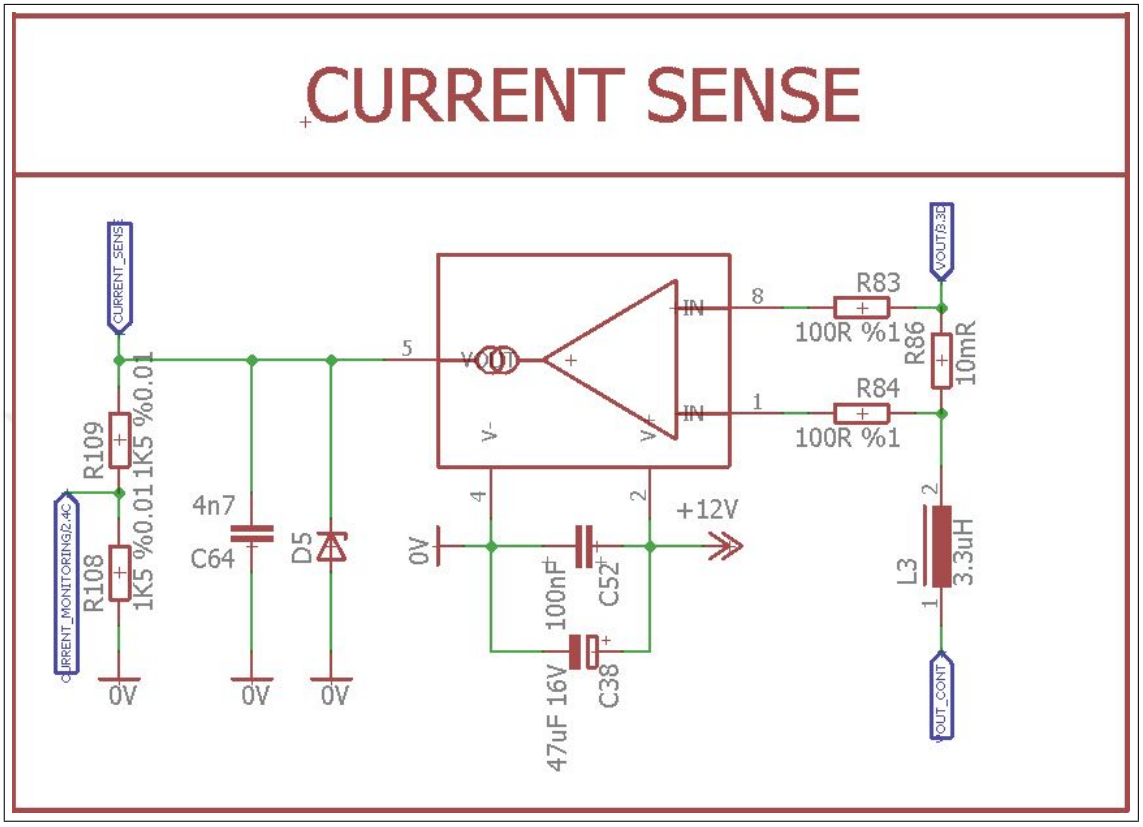


Figure 2.5 Schematics of current sense circuit.

The voltage measurement circuit is a simple voltage divider consisting of two resistors. The output voltage is divided according to the ratio of R22 to R23, where R22 is 1 MΩ and R23 is 10 kΩ. The resulting ratio is 100. In addition we measure the output voltage while consuming minimal current.

2.2.3 Current Control Circuit

MCP4921-E/SN is single channel 12-bit voltage output Digital-to-Analog Converter (DAC) operates from a single 3.3V voltage supply with an SPI compatible serial peripheral interface which is connected to the MCU [20]. The DAC output is connected to LM358 which is designed as an non-inverting op-amp. The non-inverting op-amp output is connected to the power op-amp IN+ pin. The output voltage of LM358 de-

termines the output voltage of power op-amp, so that the output current is controlled. R26, R27, R28 and R29 equals to 10kΩ. The output voltage is calculated according to the formula written below as $V_{ILIM} = V_{DAC}$.

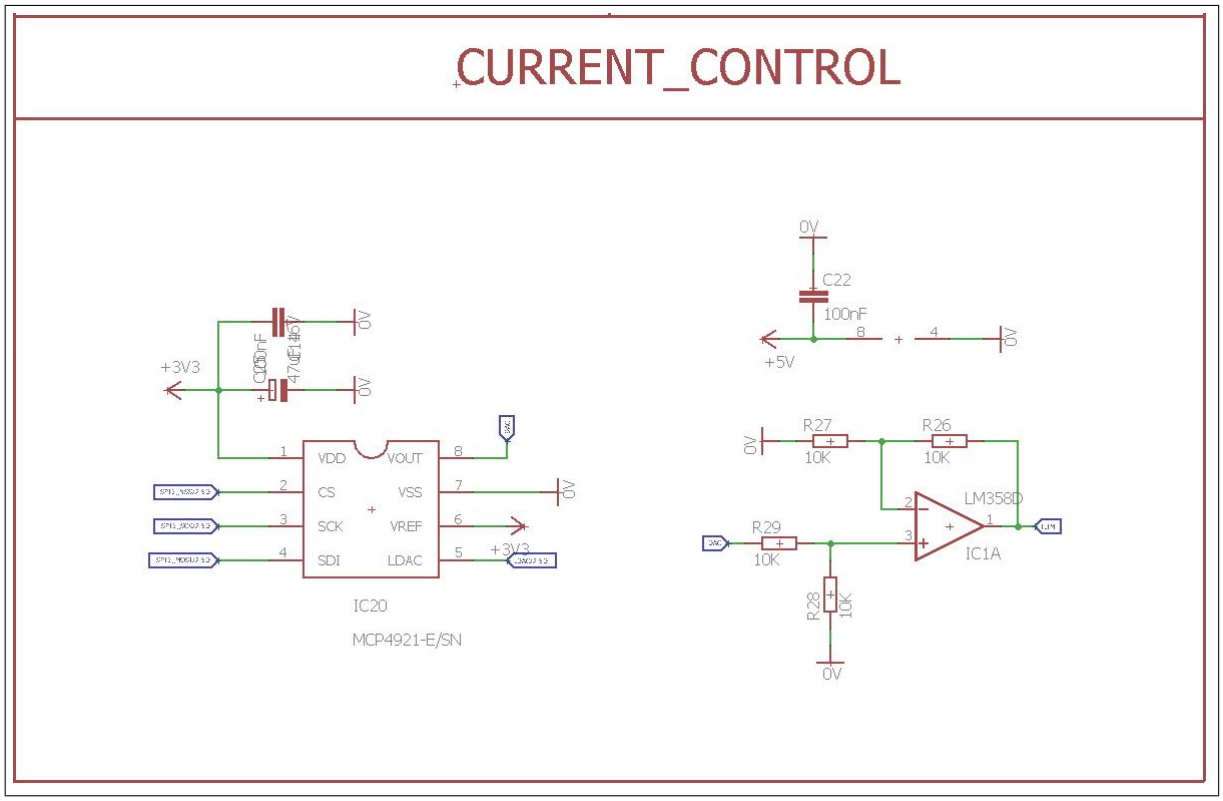


Figure 2.6 Schematics of current control circuit.

$$V_{ILIM} = (1 + \frac{R26}{R27}) \cdot \frac{R29}{R28 + R29} \cdot V_{DAC} \tag{2.3}$$

The reason I used an LM358 between the power op-amp and DAC is for the flexibility of selecting output voltage during the prototyping process, and it also provides additional isolation between the MCU and the power op-amp as seen in Figure 2.6.

2.2.4 Power OP-AMP

According to the system requirements the power op-amp was chosen as OPA549 which can supply 8A continuous and 10A peak current. The OPA549 has a wide supply range, in this case a single supply was chosen and 12V is connected. ILIM pin is connected to 0V for maximum current output and +IN pin is connected to output of LM358 op-amp. According to the current driven from the power op-amp, it generates heat, so we have mounted a large aluminum heat sink on the tab. Also the OPA549 has internal protection mechanisms against both over-temperature conditions and current overloads.

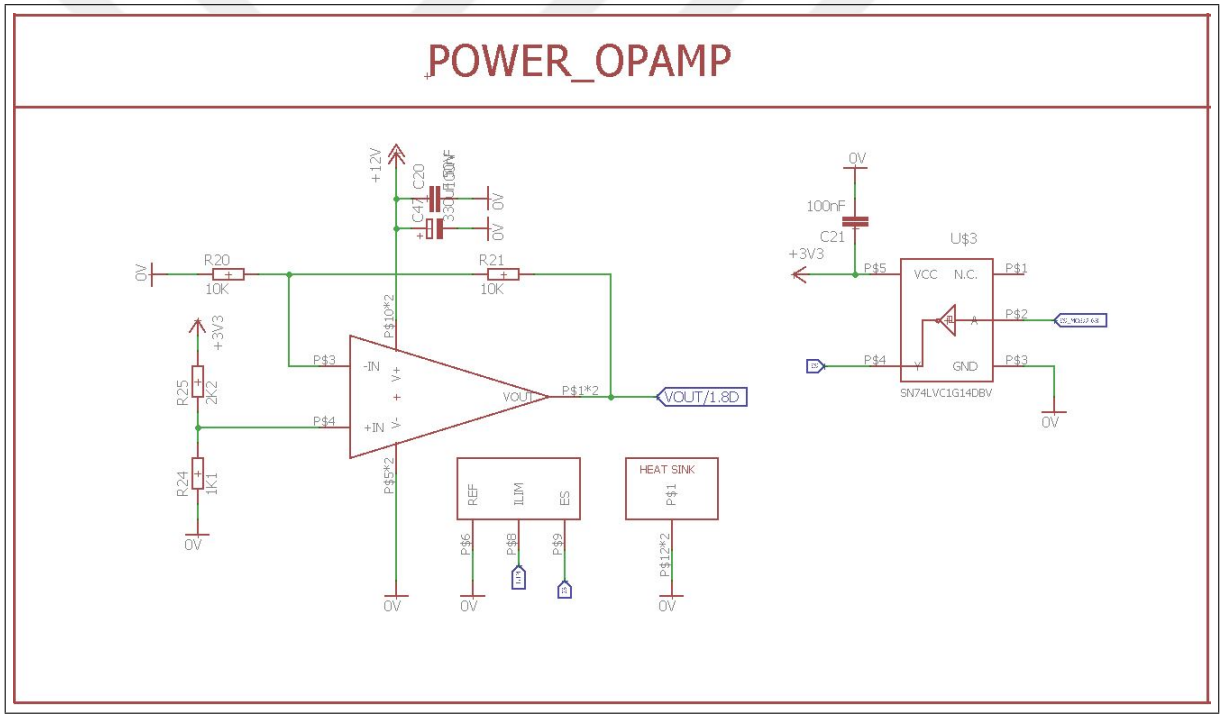


Figure 2.7 Schematics of power op-amp.

The ES pin of the power op-amp provides two functions. It can indicate thermal shut-down or it can be forced to close the output voltage. In this case I have used it to shutdown the output voltage. The output of the voltage of the non-inverting op-amp can be calculated by the formula written below; Where R21 is 10kΩ and R20 is 10kΩ, so the gain of the system is calculated as 2.

$$V_{OUT} = (1 + \frac{R21}{R20}) \cdot V_{IN+} \tag{2.4}$$

According to the gain of the system the output voltage of DAC is multiplied by 2 and the maximum output voltage of the system is the supply voltage of the power op-amp, but for safety requirements of diode laser the maximum output voltage of the system is limited to 6.8V.

2.2.5 Power Supply

The power supply of the ECU consists of step-down (buck) switching regulator and linear regulator. The buck regulator of the board is connected to power unit of the system and the output of the buck regulator is connected to the input of linear regulator. The 12V input voltage is regulated to 5V by the buck regulator and 5V is reduced to 3V3 by linear regulator. LM2596-ADJ is selected as the buck regulator, it can supply 3A continuous output [21]. The fuse and varistor located at the voltage input provides additional electrical safety for the system. The linear voltage regulator connected in parallel provides a continuous 3A 3V3 output, with each regulator supplying 1.5A.

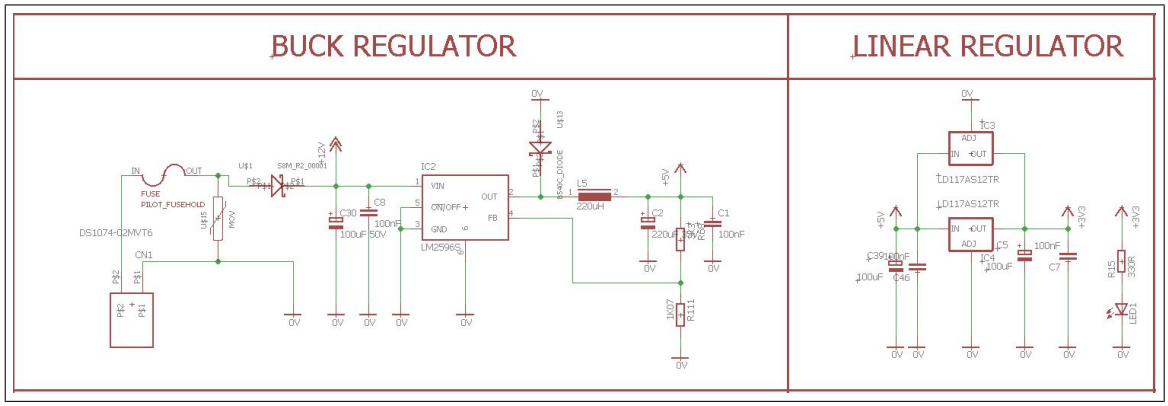


Figure 2.8 Schematics of the power supply of electronic control unit.

$$V_{OUT} = V_{Ref} \cdot (1 + \frac{R68}{R111}) \tag{2.5}$$

The output voltage was calculated by the formula written above; where V_{Ref} equals to 1.23, R68 is selected 3.3kΩ and R111 is selected as 1.07kΩ. The calculated output voltage would be 5.02V.

2.2.6 Microcontroller Unit

The MCU selection of the ECU unit was the one of the most important step of prototyping process. Selecting a fast, reliable, cost effective and well-documented MCU that includes the required peripherals was important. Additionally, pin-to-pin replacement capability in case of misselection during development was crucial. As a consequence we have selected STM32F446RCT6 as the MCU of the system. Some important features and peripherals of the MCU are written below [22];

- ARM Cortex-M4 STM32F4 Microcontroller
- 32-Bit Single-Core 180MHz operating frequency
- 256KB (256K x 8) FLASH program memory
- CANbus, EBI/EMI, I2C, IrDA, SPI, UART/USART, USB, USB OTG wide range connectivity
- 12-bit ADC up to 24 channels of analog inputs
- SWD and JTAG interfaces Debug mode
- 64-LQFP (10x10) Package

ST Microelectronics STM32F446RCT6 MCU enables us to work with variety of software development environments such as IAR, Keil and STM32CubeIDE. Since

IAR and Keil are better compilers for code optimizations, it requires license for ARM Cortex-M4. On the other hand STM32CubeIDE requires no license for any ST Microelectronics MCU, but code optimizations are slightly inferior which results using more program memory. Fortunately, we have large memory space, so the slightly worse code optimizations are negligible so that we have chosen STM32CubeIDE for software development.

2.2.7 Communication Interfaces

Electronic control unit is the core of the system and requires variety of communication interfaces. In this prototype we have designed RS-232, RS-485 and USB interfaces which can support 115kbps baud rate. For the RS-232 serial communication interface, we utilized the MAX3232IDR , a 3-V to 5.5-V multichannel RS-232 Line Driver/Receiver [23]. This low-cost and widely accessible IC is directly connected to the UART of the MCU.

For the RS-485 half-duplex communication IC, we have chosen MAX3485EESA harsh environment integrated circuit [24]. The supply voltage of this IC is within the limits of MCU supply, so that we have directly connected to the UART of the MCU. This interface have not yet used for this project, but reserved for future use.

For the USB interface, we have used CP2104 USB-TO-UART bridge. Silicon Labs, the manufacturer of this IC, provides virtual com port drives for variety of operating systems including Windows, Linux and Mac OS-X which enables the system to work with existing com port PC applications [25]. The small QFN-24 package of the IC on the other hand provides PCB space. The supply voltage of this IC is within the limits of MCU supply, so that we have directly connected to the UART of the MCU.

2.2.8 PT-500 Temperature Measurement Circuit

During laser output control, the power op-amp generates excessive heat, which may lead to undesired outcomes such as misregulation of output voltage, thermal shutdown, or circuit breakdown. The PT-500 temperature measurement of the power op-amp provides real-time surface temperature readings. The algorithm checks if the system is operating within healthy parameters and intervenes if it exceeds predefined limits. Therefore we have designed the fallowing circuit and connected to the ADC of the MCU.

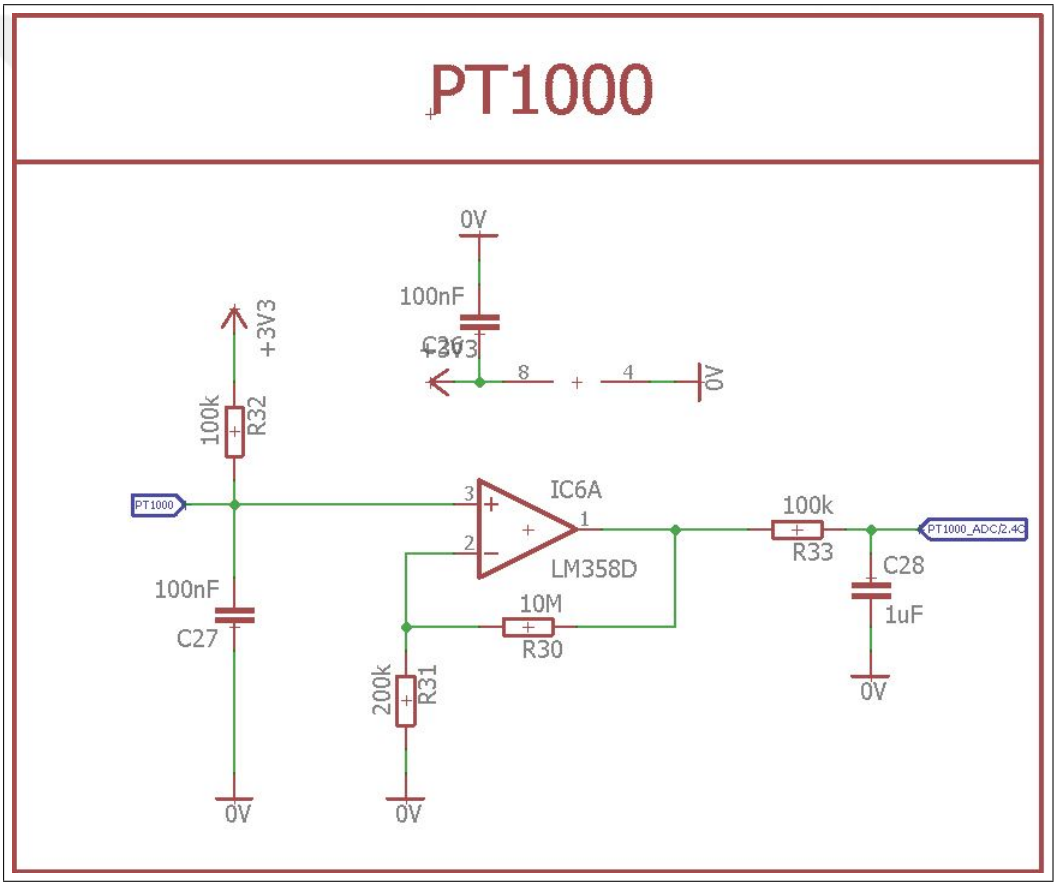


Figure 2.9 Schematics of PT-500 temperature measurement circuit.

Initially, we designed the circuit for a PT-1000, which could provide a measurement resolution of 0.1 degrees Celsius. However, we ended up purchasing a PT-500 instead, which offers a resolution of 0.2 degrees Celsius, but it is still sufficient for the system's needs. The circuit is basically a non-inverting amplifier. As the temperature changes, the resistance in the PT500 also changes, leading to a corresponding out-

put change in the op-amp. According to the measured output voltage the algorithm calculates the surface temperature of power op-amp.

2.2.9 Other Peripherals

For practical usage and user-friendly reasons, the ECU includes a buzzer, LED indicators for communication, and thermal jumpers for transferring heat and electrically isolating components.

2.2.10 Electronic Control Unit PCB Design

Two-layer PCB design was preferred as an inexpensive solution. The PCB material was chosen as FR4 for higher temperature durability and the enclosure material was chosen as aluminum for heat dissipation. AL-115-15 code written on top of the Figure B.1 shows the manufacturer product number of the enclosure. Blue lines indicate bottom layer and red lines indicate top layer. Moreover green holes indicate vias and pads that connects top and bottom layer. The PCB properties are written below;

The PCB properties:

- Material: FR-4 TG150
- Layer: 2 Layers
- Finished copper: 35um
- Thickness: 1.6mm
- Surface finish: HASL with lead
- Size: 100.4 x 149.8 mm

Connectors CN2, CN3 and X6 are communication interfaces. The connector CN1 is the power input of the device and the input voltage of the device is 12V. CN5 is the connector for the laser fan, laser diode and PT-500. The fuse is 3A 5x20 glass and easily replaceable. The two 3.5mm holes located at the center of the board are intended for PCB support, preventing the PCB from bending. Remaining connectors on the PCB were reserved for future use.

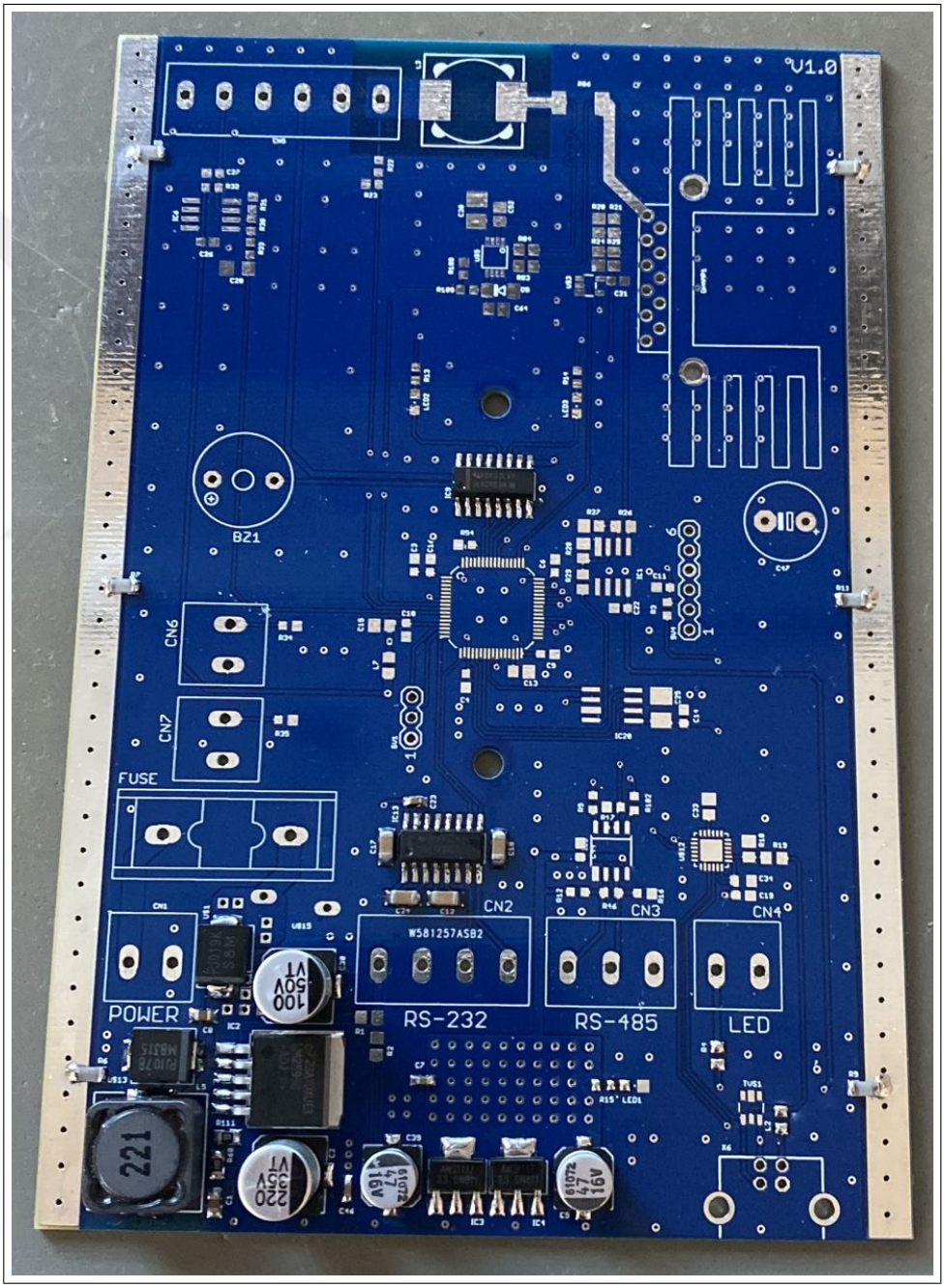


Figure 2.10 Printed circuit board of electronic control unit.

Manual changes made on the PCB during the design validation:

1. Resistor R86 case was insufficient in terms of watt, changed with 5W 5mΩ resistor.
2. OPA549MKVC was warmed up more than expected, the aluminum heat sink of the power Op-Amp changed with a bigger one.
3. USB lines D+ and D- was connected reverse, the lines were cut and connected properly.
4. OPA549MKVC Op-Amp ILIM pin connection with LM358 Op-Amp were cut and ILIM pin was grounded for max. current output.
5. OPA549MKVC IN+ pin connected to LM358 Op-Amp.

2.3 IR Array Unit

IR array unit consists of 5 main sections as seen in Figure 2.12. These are positioning laser, IR Array module, MCU, and communication interfaces, respectively. The IR array module communicates with MCU via I2C, and the temperature values of 32x32 pixels measured at 330ms intervals are transmitted to the MCU.



Figure 2.11 The 650-nm 5mW positioning laser.

The instantaneous surface temperature information is obtained, and the average of the temperature values of 4 pixels located at 15th row-15th column, 16th row-15th column, 15th row-16th column, and 16th row-16th column in the center is calculated. This average temperature information is then sent to the ECU via RS-232 at a speed of 115200bps. On the other hand, the RS-485 communication interface is connected to the PC. The temperature information of 32x32 pixels is responded at a speed of 115200bps upon the command received from the PC, and it is displayed on the interface program.

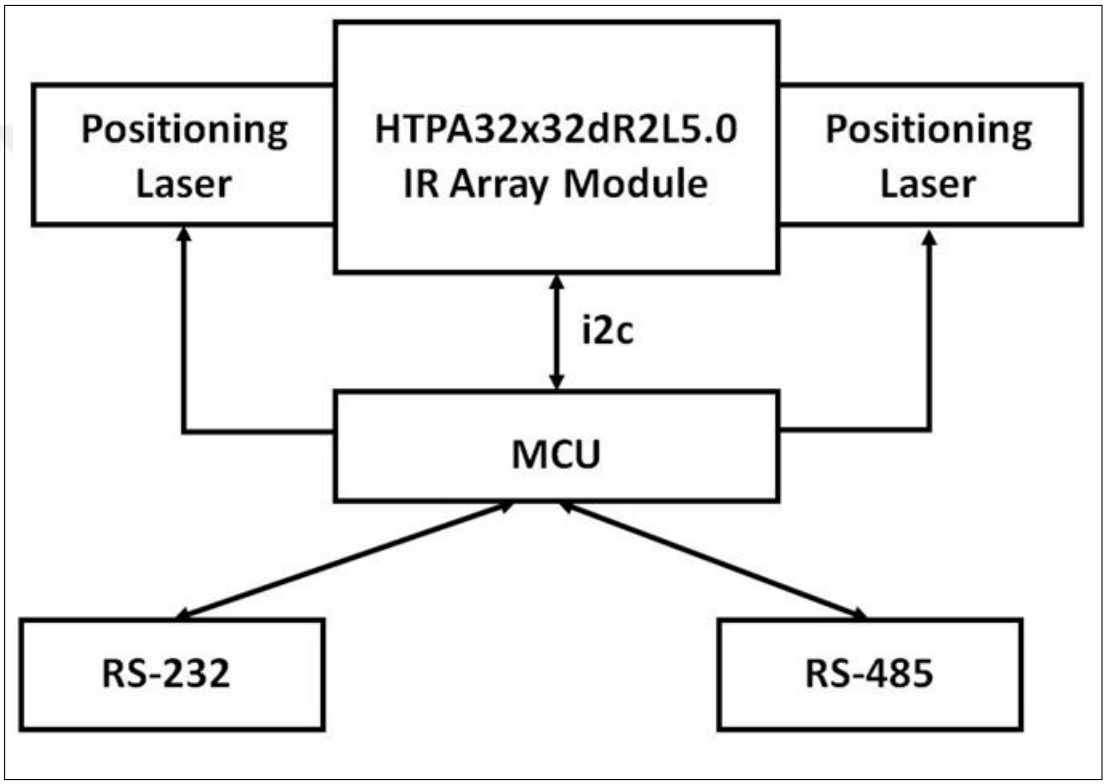


Figure 2.12 Block diagram of IR Array Unit.

The positioning lasers are 5mW 650nm dot lasers as seen in Figure 2.11 and placed at the both sides of IR array module. The main purpose of these lasers is to facilitate the usage of the IR array unit during experiments. The positioning lasers toggle in every 1s and the pointed area is the location where IR array unit measures. RS-232 serial communication, RS-485 circuit and power layers are identical with the electronic control unit as seen in APPENDIX A and APPENDIX B. Moreover, the MCU used in the IR array unit, with a core speed of 180 MHz and connectivity capabilities, is identical to the one used in the ECU.

Table 2.1
The factory default configuration of the HTPA32x32dR2L5.0 Heimann Sensor IR Array module.

Trim_Registers	Settings	Binary Expression
MBIT_TRIM	16 bit ADC Resolution	0010 1100
BIAS_TRIM_TOP	12uA	0000 0101
BIAS_TRIM_BOT	12uA	0000 0101
CLK_TRIM	4.33MHz	0001 0101
BPA_TRIM_BOT	0.4uA	0000 0011
PU_SDA_TRIM	100kΩ	1000 1000

The selection of the thermopile array sensor was the core of the IR array unit design. According to related studies [26], we have selected the Heimann Sensor HTPA32x32dR2L5.0, which offers a 32x32 pixel resolution with a framerate of 2Hz to 27Hz and 33 degree focus of view [27].

2.3.1 Design Considerations

Choosing electronic components according to system requirements is crucial for ensuring optimal performance and functionality. Factors such as power consumption, processing speed, interface compatibility, size, and cost need to be carefully considered during the selection process.

The first step was deciding between an IR sensor or IR array sensor. The IR sensor provides an output of the average measurement value of the targeted area. If the area measured by the IR sensor is larger than the region where the laser emits radiation, an incorrect measurement result would have been obtained since the average temperature measurement is provided as the output.

On the other hand, an IR array sensor measures the focused area and provides output values for individual pixels. By measuring small portions of the targeted area, we were able to determine the size of the laser beam spot. Therefore selecting an

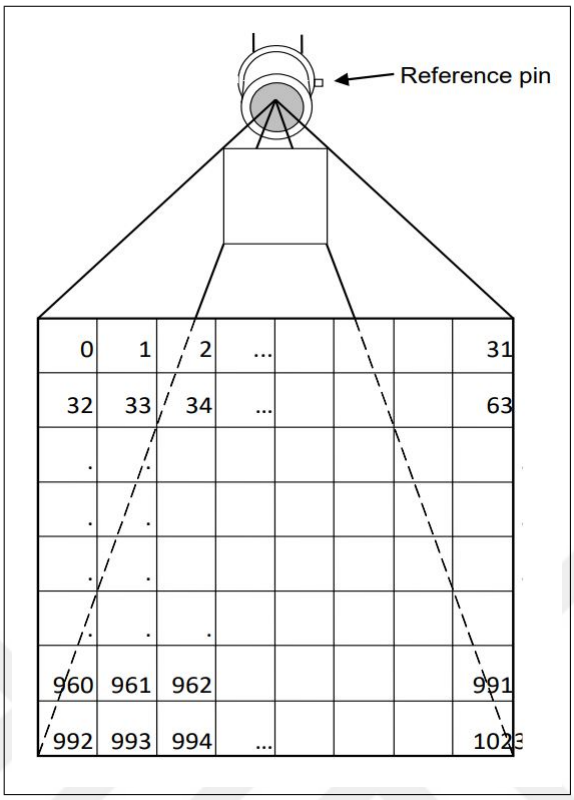


Figure 2.13 The Heimann Sensor HTPA32x32dR2L5.0 pixels.

IR array sensor would be advantageous for the system. However Heimann Sensor detailed datasheets and module library was not open source and we had to contact the manufacturer directly to develop our system. During the development process, we discovered that the factory default configuration of the module provides the most accurate temperature values, which is set to 3 FPS, as strictly recommended by the manufacturer.

2.3.2 IR Array Module Design

Schematics for an IR array unit designed to meet physical requirements, including the FOV of the IR array module and the aluminum enclosure. The daughterboard is assembled with positioning lasers and the HTPA32x32dR2L5.0 module. The motherboard includes a connector that connects to the daughterboard. The peripheral resistors and capacitors added according to datasheet of the sensor [27].

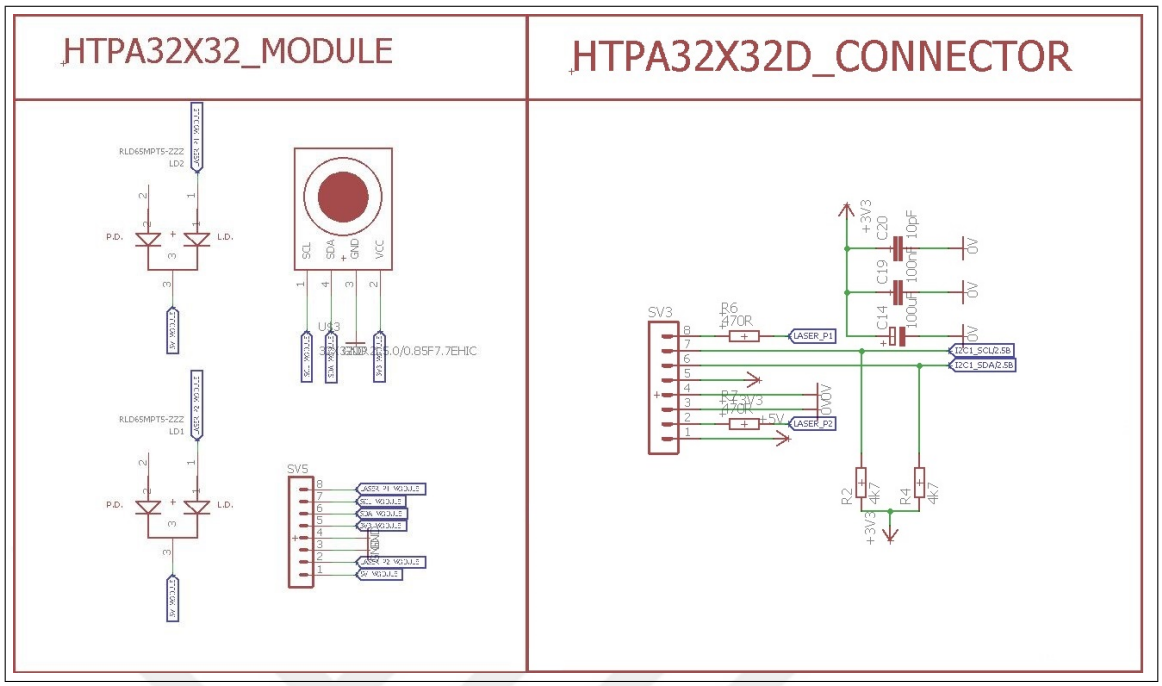


Figure 2.14 Schematics of The Heimann Sensor HTPA32x32dR2L5.0 module.

The sensor connectivity is through I2C and connects to the I2C port of the MCU as seen in APPENDIX C and APPENDIX D. The module is supplied with 3.35V and C14 was chosen as tantalum capacitor which can supply rush current. C19 and C20 are 100nF and 10pF respectively, added for noise filtering. The positioning lasers are connected to ULN2003A darlington transistor array [28] through resistors R6 and R7. The bases are connected directly to MCU IO and configured as output. The voltage supply of lasers are both 5V.

2.3.3 IR Array Unit PCB Design

A two-layer PCB design was preferred as a cost-effective solution. The PCB material selected was FR4 for its physical durability, while aluminum was chosen for the enclosure material to enhance durability further. AL-053 code written on top of the Figure 2.15 shows the manufacturer product number of the enclosure.

Connectors X1 and X4 serve as communication interfaces. Additionally, SV3 is designated for the IR module daughterboard. The connector X5 is the power input of

the device and the input voltage of the device is 12V. Connector SV4 is a male 2.54mm pin header for debugging and programming the MCU.

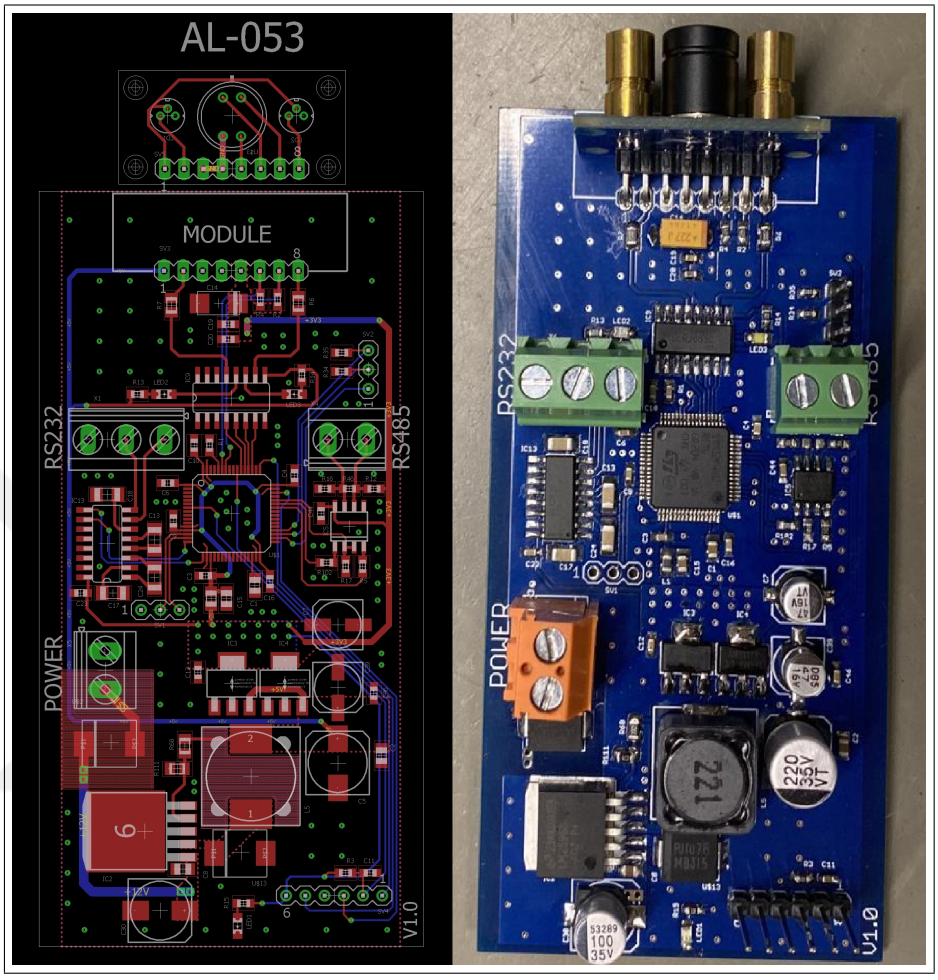


Figure 2.15 Design of the printed circuit board of IR array unit and the assembled PCB

The PCB properties:

- Material: FR-4 TG150
- Layer: 2 Layers
- Finished copper: 35um
- Thickness: 1.6mm
- Surface finish: HASL with lead
- Size: 50.8 x 99.8 mm and 30 x 15 mm

2.4 Installation of The System

The system consists of a power unit, an Electronic Control Unit (ECU), an Infrared (IR) array unit, and an 808nm laser. Utilizing a 20x20 mm sigma profile structure was convenient for the integration of all system components. The laser's focal point was 22cm, aligning perfectly with the adjustable height experiment platform measuring 20x20 cm. The power unit and ECU dimensions also considered for the sigma profile structure, ensuring compactness and efficiency as well as cost effective solution.

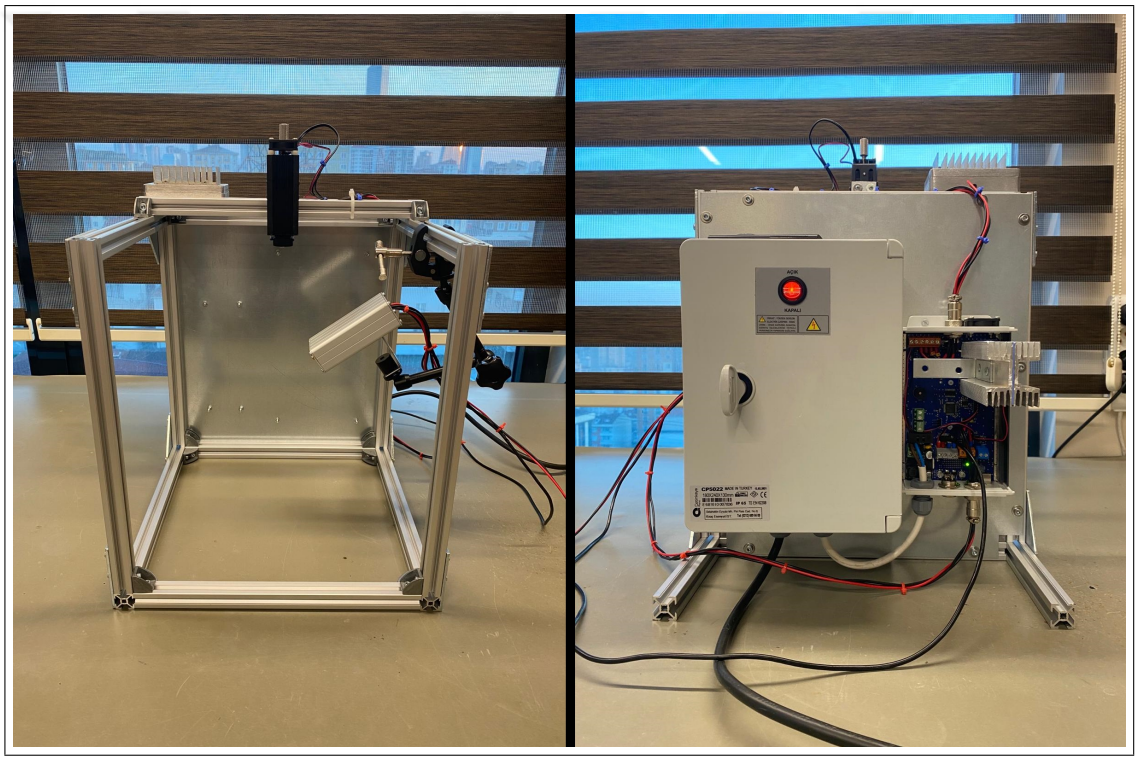


Figure 2.16 Front and rear view of the system

To maintain equilibrium, the ground sigma profile was chosen with dimensions of 48cm, 36cm in height, and 30cm in width, ensuring alignment with the system's center of gravity. The power unit and ECU are installed at the rear of the structure, with the laser positioned at the center, while the IR array unit is mounted onto the adjustable camera arm, as depicted in Figure 2.16.

2.5 User Interface

The user interface program Hercules is free software that can be downloaded from the internet. Hercules freeware supports serial port terminal (RS-485 or RS-232 terminal), UDP/IP terminal and TCP/IP Client Server terminal. In this project we particularly used the serial port terminal ability. The communication parameters between ECU and PC were set as 115200 baud rate, data size 8 and parity as none.

The measured parameters can be monitored real-time such as IR array sensor measurement, current through the laser diode, output voltage and power op-amp temperature. Moreover three types of commands can be given from Hercules.

The command examples are written below;

- *123:MODE:480000:42.5##
- *123:CLOSE##
- *123:OPEN:30000:89##

The commands starts with * and ends with # signs. The following three digit number is the command id and can be changed by the user. The command CLOSE instantly shuts off the system The command OPEN starts laser irradiation only. The following number defines the operation duration in terms of milliseconds and last number defines the output percentage of the laser. The command MODE starts operation conditionally where the following number in the command defines the operation duration in terms of milliseconds and last number defines the targeted surface temperature. The laser irradiates at 100% until the measured value reaches the targeted value. After reaching the targeted value, system adjust the laser output and keeps the measured temperature at targeted value. The operation is terminated when it reaches the predefined time value.

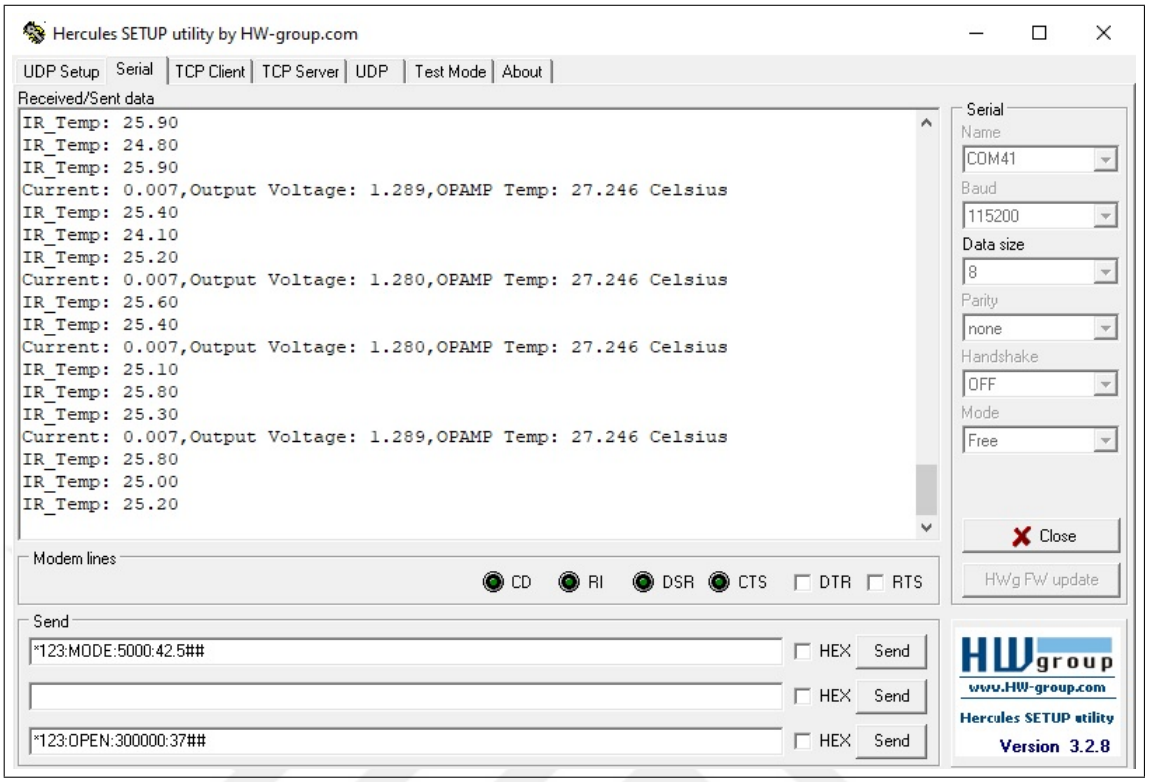


Figure 2.17 User interface program.

2.6 Power vs Laser Diode Current

The output power of the laser system was measured using power meter (Newport power meter model 1918-R). The laser diode has a threshold of 1 A, and 10 measurements were taken between 1 and 5 A by the power meter. The output power of the 808-nm laser system with respect to current is plotted due to the measurements. The graph depicts a nearly straight-line trend. However according to the manufacturer of the diode laser, at 5A we were expecting 5W of output power, but we had measured 3W instead.

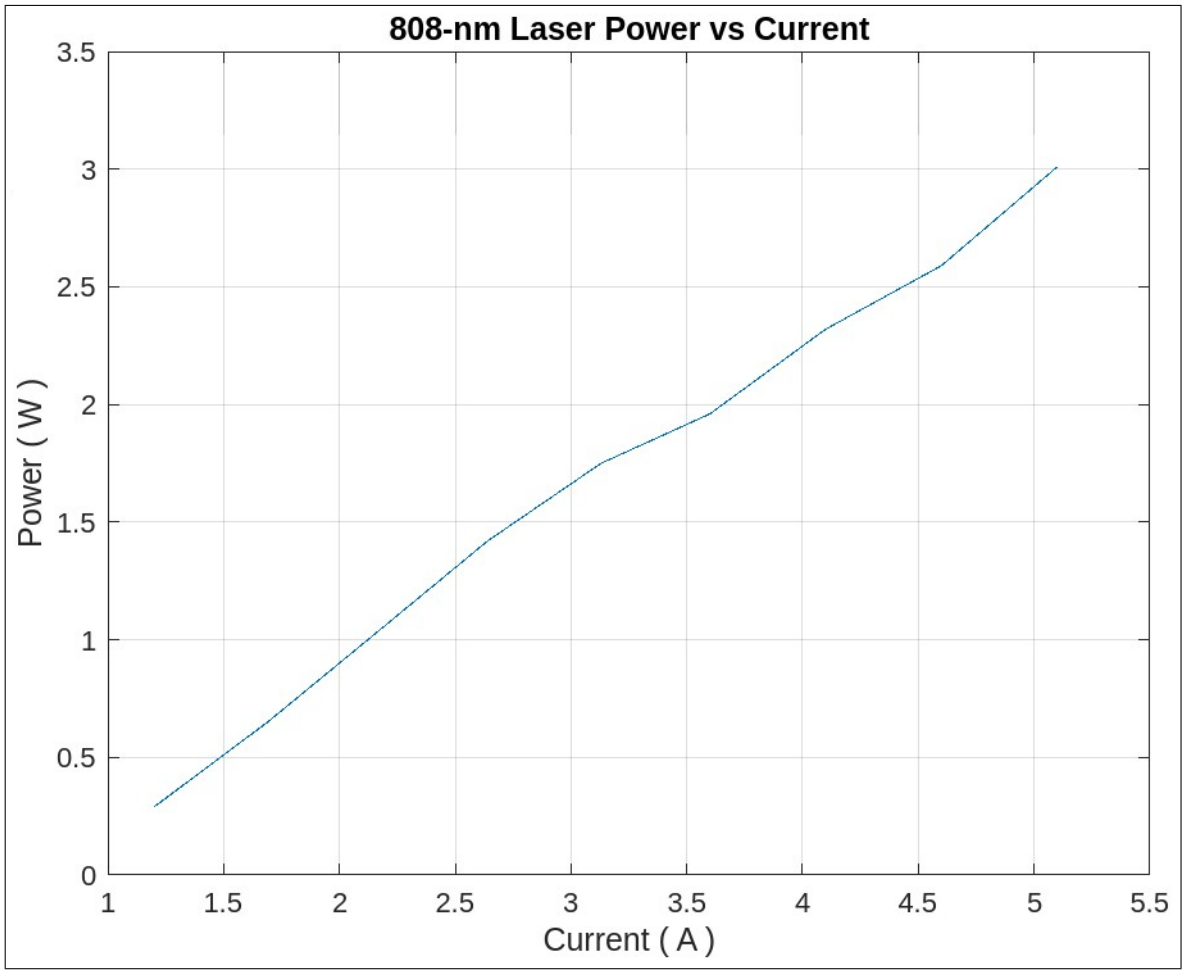


Figure 2.18 Laser output power vs current.

3. METHODS

3.1 Temperature Measurement Using the IR Array Sensor and Comparison with a Commercial IR Thermometer

An infrared (IR) array sensor the HTPA32x32dR2L5.0 model from Heimann Sensor GMBH, was purchased and utilized in its factory-calibrated state. To assess the sensor's measurement precision, temperature readings of ice, room-temperature water, and boiling water were taken using the aforementioned IR array sensor. These measurements were then compared with readings obtained from a Raytek Raynger ST IR thermometer.



Figure 3.1 Raytek Raynger ST IR thermometer.

The measurements obtained from the IR array unit consisted of a 32x32 pixel array, with each reading averaging across 1024 pixels. In contrast, the commercial IR thermometer provides output for a single-pixel measured area, where the average temperature is determined. For a more accurate comparison, efforts were made to measure the same area according to the field of view (FOV) of both devices.

3.2 Temperature-Controlled Laser System Flowchart

As shown in the flow chart in Figure 3.2, the experiment loop starts with the command given by the PC. The loop refreshes itself after receiving temperature data from the IR array sensor, around every 350 ms. During the loop, the measured sample temperature (average of four pixels located at the center of 32x32 pixel data) is compared with the target temperature. If the difference between the measured temperature and target temperature is smaller than -1.0°C (i.e., the sample temperature < 41.5°C), the current, therefore the laser output, was set to 100%, which refers to 3W. If the difference between the measured temperature and the target temperature is larger than 0.6°C (i.e., the sample temperature > 43.1°C),the current was set to a lower value so that the output power decreases. Specifically, for agar gels, the output power was set to 40%. Due to the rapid temperature increase in liver tissue, this value had to be taken as 20% for liver tissue. For the temperatures that are outside the abovementioned conditions, the formula "Laser Output Set = [80 - Temperature Difference x 50]" was applied for agar gels, and "Laser Output Set = [50 - Temperature Difference x 50]" was applied for liver tissues.

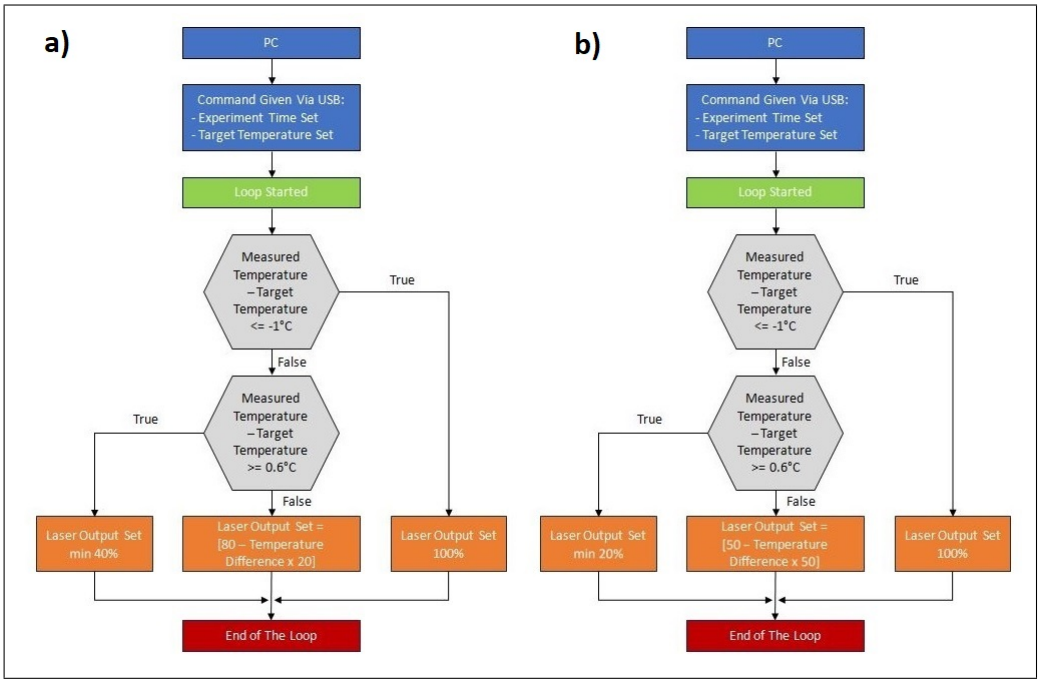


Figure 3.2 (a) Laser control flowchart for agar gel irradiation. (b) Laser control flowchart for lamb liver irradiation.

The current and voltage information from the laser diode, as well as the data from the IR array sensor, were instantly transmitted to the PC to display on the interface program and log during the experiment. Additionally, the system was designed to be able to obtain a 32x32 pixel image during irradiations via the direct connection between the IR array sensor and the PC.

3.3 Preliminary Studies

Agar gel was prepared by dissolving 40 g of agar powder in 1l of distilled water and poured into 100 mm Petri dishes to obtain gels of around 5 mm thickness. The samples were irradiated using the temperature-controlled laser system that was set to 42.5°C. Irradiations were terminated after the temperature of the samples were kept constant for around 5 minutes. The experiment was repeated three times. The temperature change over time for one repeat was shown in the Results section. The box and whisker plot of the temperature change for the same repeat was provided in Figure 4.3 (a).

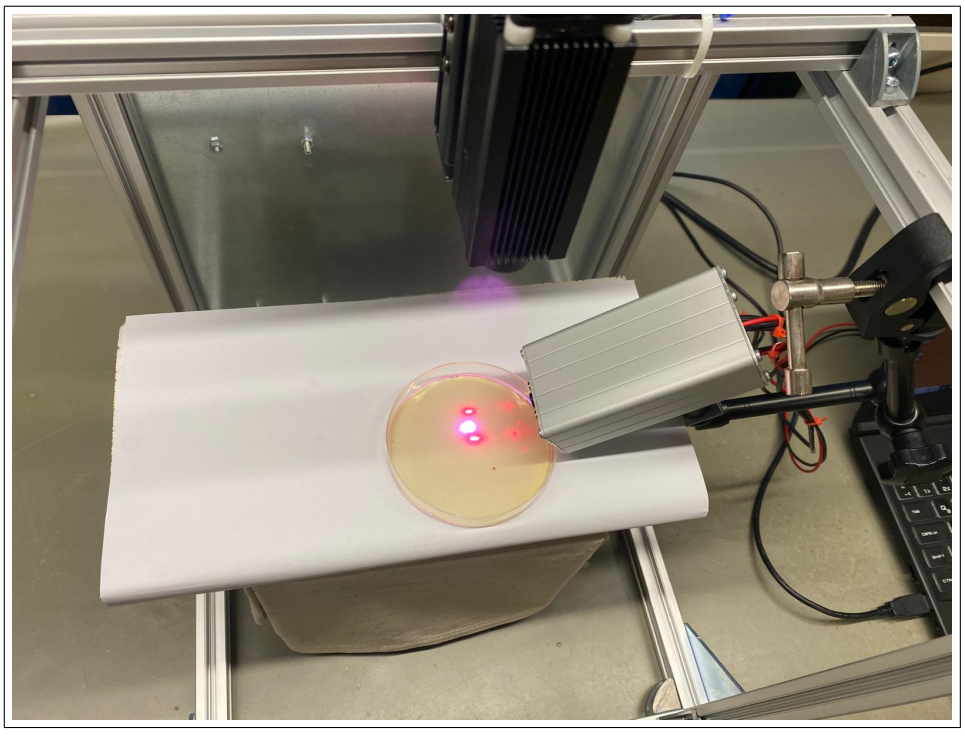


Figure 3.3 Agar gel experiment setup.

Fresh lamb liver was obtained from a local butcher and samples with thicknesses of 6-7 mm were prepared before the experiments. The samples were kept in saline during the experiment and irradiated using the temperature-controlled laser system set to 42.5°C. Irradiations were terminated after the temperature of the sample was kept constant for around 5 minutes. The experiment was repeated three times. The temperature change over time for one repeat was shown in the Results section. The box and whisker plot of the temperature change for the same repeat was provided in Figure 4.3 (a).

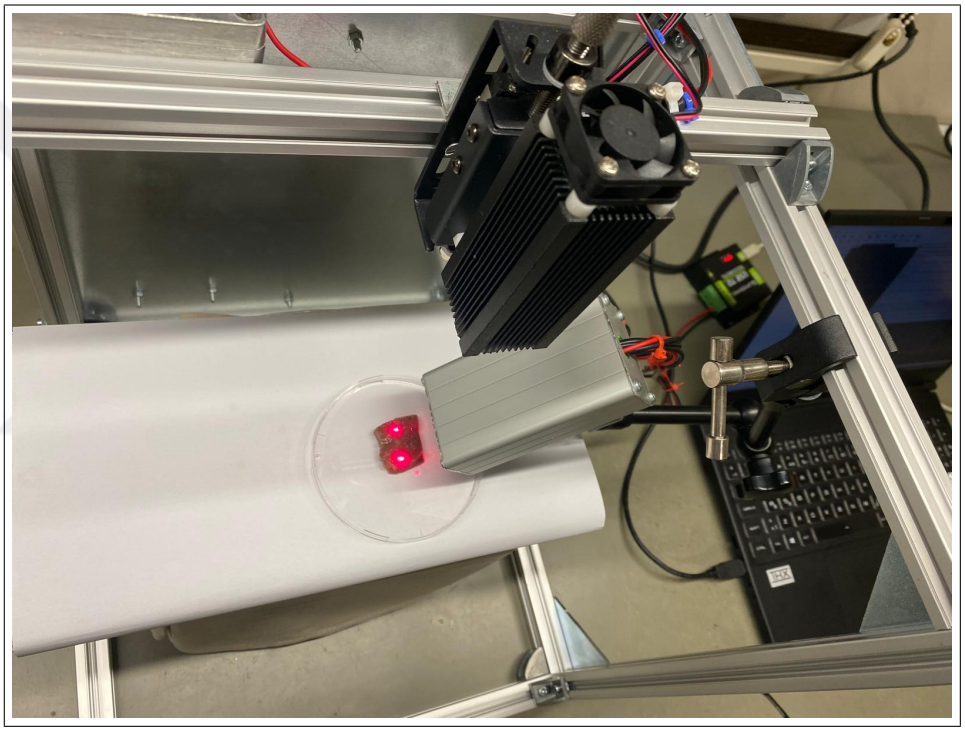


Figure 3.4 Lamb liver experiment setup.

Lamb liver tissues were irradiated under two conditions: one with temperature control and the other with a constant power setting. This was conducted to compare the outcomes between the two approaches. The irradiated laser power was determined from the outcomes of the temperature-controlled experiment by integrating the current versus time data. The constant laser power experiment was conducted three times. The temperature change over time for three repeat was also shown in the Results section.

3.4 System Improvements

Even though the same laser energy is applied to different tissue types, the rate of temperature increase in the tissues varies according to their optical properties. As seen in Figure 3.2 two different algorithms applied to two optically different samples. If the algorithm designed for agar gel had been applied to the lamb liver experiment, the tissue would have burned. On the other hand if the algorithm of lamb liver would had applied for agar gel, we could not reach the targeted temperature value. It is because the FPS (frames per second) of the IR Array Module is not fast enough to detect surface temperature and generate an outcome.

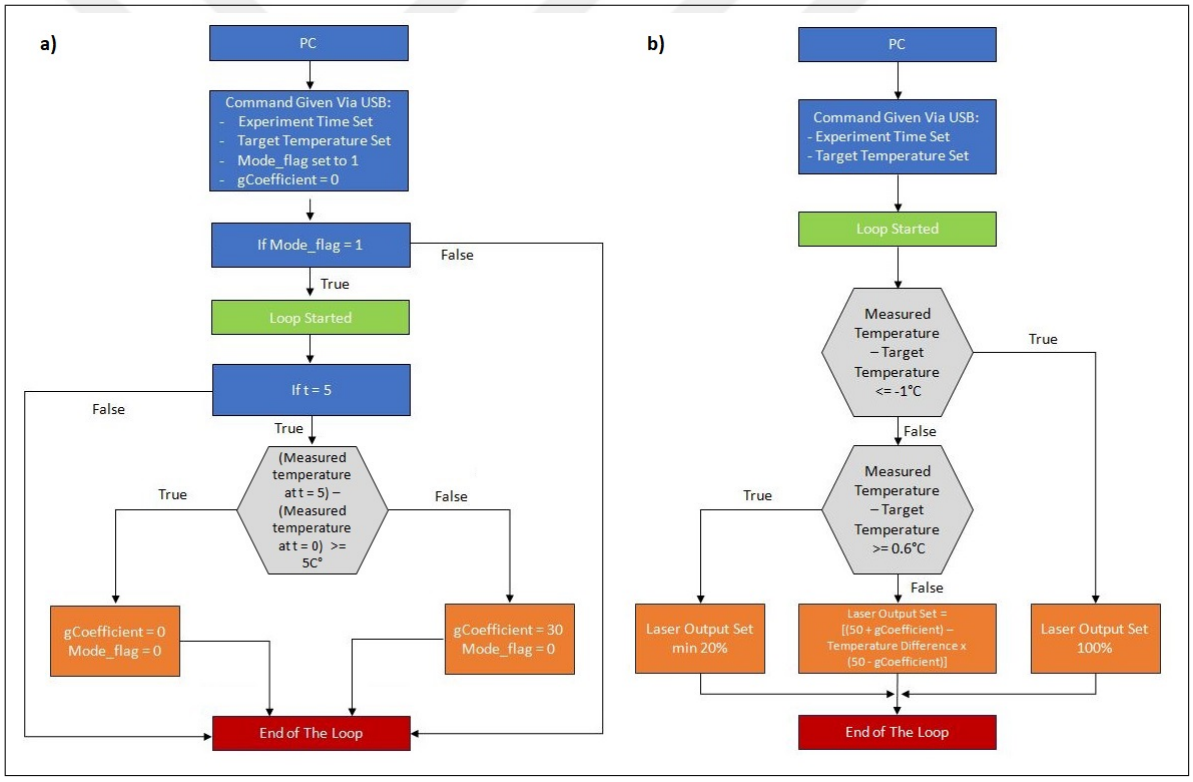


Figure 3.5 (a) Flowchart of temperature detection rate function. (b) Updated flowchart of laser irradiation control.

We have observed that within the first 5 seconds, the rate of temperature increase varies according to the optical properties of the samples. Based on this observation, we have developed an algorithm, as seen in Figure 3.5a.

The temperature increase rate detection function runs in the system timer module of the MCU, which operates simultaneously with the main program. The function remains idle until a command is received from the PC. Upon receiving the command, the mode flags are set to one and the time counter starts. At "t=0," where t represents seconds, the first temperature measurement is recorded, and at "t=5," the last measurement is recorded. The gCoefficient variable is then set based on the difference between these two values. If the difference is higher than 5°C, the gCoefficient remains the same, which is zero; otherwise, the gCoefficient equals 30. The mode_flag variable is set to zero in either case, and the function remains idle until another command is given.

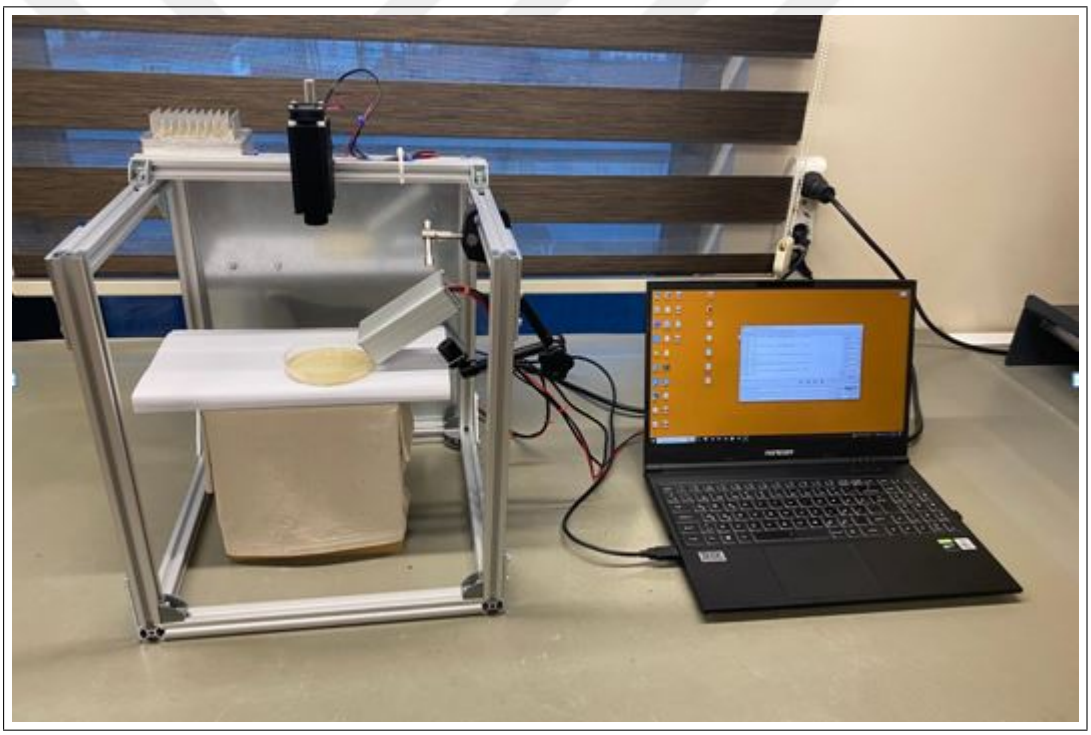


Figure 3.6 Temperature-controlled laser system setup.

The updated flowchart of laser output control, as seen in Figure 3.5b, runs exactly the same as the flowchart seen in Figure 3.2b, with the only difference of the gCoefficient variable. At the beginning of the loop, the gCoefficient variable is set to zero. At the fifth second of the loop, the coefficient is either set to 0 or 30, and the variable remains the same until the end of the designated experiment time. The system detects the tissue type and apply the convenient algorithm of laser irradiation control.

3.5 Photothermal Applications

Agar gel experiment was repeated following the same procedure mentioned in Section 3.3 to ensure that the updated algorthm works as expected. During the experiment, temperature increase rate detection function was monitored through the debug port of the MCU. The temperature change over time for one repeat and heat map was shown in the Results section. The box and whisker plot of the temperature change for each experiment was provided Figure 4.6.

The vertical and horizontal field-of-view were calculated based on the target distance, viewing angle and angular FOV, where distance is 25mm, viewing angle is 49 and FOV is 33° respectively. According to the trigonometric calculations as seen is Figure 3.7 the width and height was calculated as 0.6565 mm.

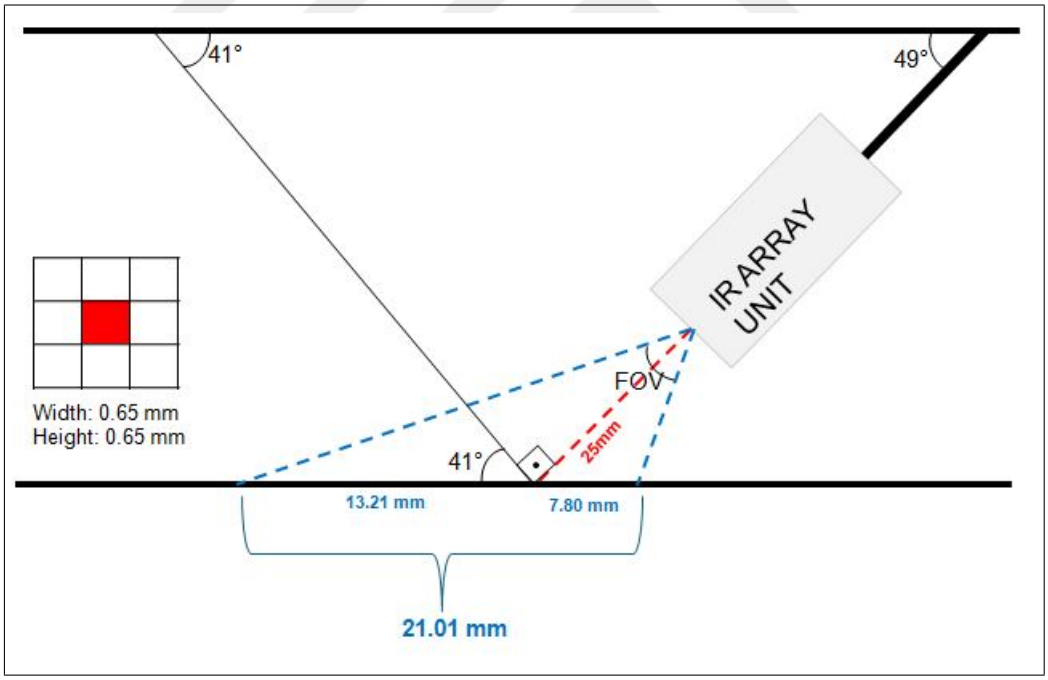


Figure 3.7 FOV calculation according to viewing angle and target distance.

Lamb liver samples were prepared by following the same procedure mentioned in Section 3.3. The samples were irradiated using the temperature-controlled laser system that was set to 50°C, 60°C and 70°C respectively. Three experiments were conducted for each temperature value. The temperature change over time for one repeat and heat

map was shown in the results section. The box and whisker plot of the temperature change for each experiment was provided in separate figure.

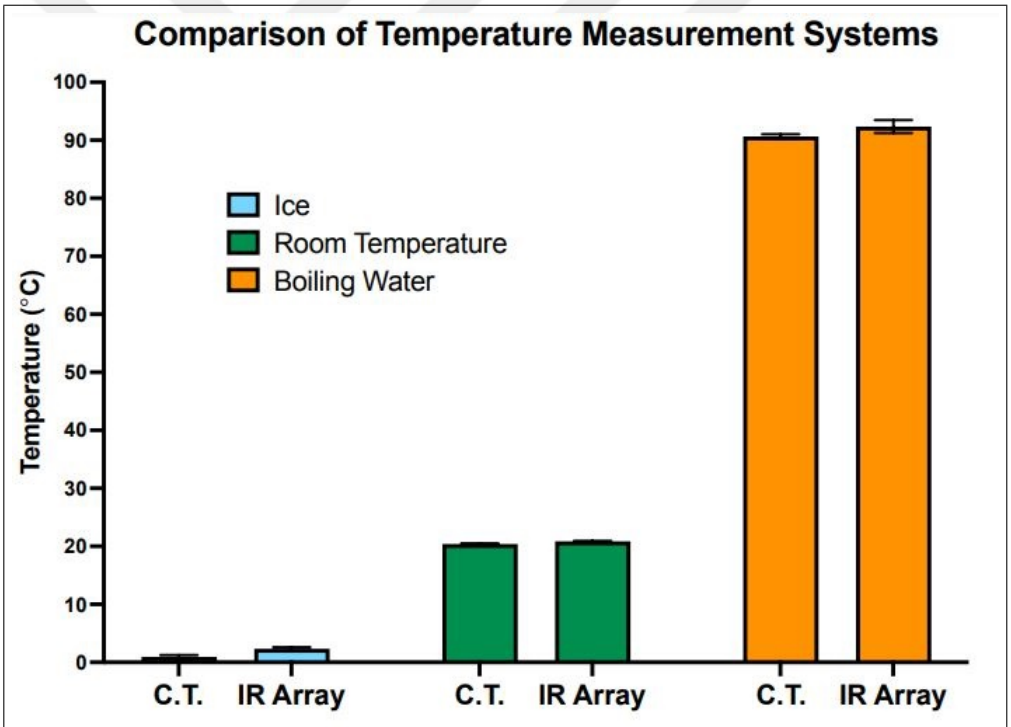
Lamb liver tissues were irradiated under two conditions: one with temperature control and the other with a constant power setting. This was conducted to compare the outcomes between the two approaches. The irradiated laser power was determined from the outcomes of the temperature-controlled experiment by integrating the current versus time data. The constant laser power experiment was conducted three times. The temperature change over time for each experiment was also shown in the Results section.

The experiments were conducted three times and shown in the Results section. The graphs were drawn by MATLAB and Prism-GraphPad programs. In addition, heat maps were drawn by MATLAB specifically.

4. RESULTS

4.1 Comparison of IR Array Sensor with a Commercial IR Thermometer

The measurement of the purchased IR array sensor was compared with a commercial handheld IR temperature measurement on ice, water at room temperature, and boiling water. According to the results, the temperature values measured by the IR array sensor are comparable with the commercial IR thermometer (Figure 4.1).



Condition	Ice		Room Temp.		Boiling Water	
Measurement Technique	C.T.	IR Array	C.T.	IR Array	C.T.	IR Array
Average of the measurements	0.96	2.33	20.4	20.86	90.66	92.37
St. Dev.	0.31	0.29	0.13	0.10	0.38	1.12

Figure 4.1 Comparison of IR array sensor with a commercial IR thermometer(C.T.).

Table 4.1
Measurement results of IR array sensor and commercial IR thermometer (C.T.) in terms of °C degree Celsius.

ICE		ROOM		BOILING	
C.T.	IR Array	C.T.	IR Array	C.T.	IR Array
1.20	2.69	20.40	21.06	91.40	94.12
1.40	2.70	20.40	20.98	91.20	93.97
1.20	2.44	20.40	20.78	90.80	93.09
1.20	2.50	20.60	20.89	90.60	92.77
0.80	2.53	20.40	20.8	90.40	92.50
0.80	2.34	20.20	20.86	90.60	92.12
1.00	2.21	20.40	20.76	90.40	91.69
0.40	1.96	20.60	20.86	90.60	91.40
0.60	2.05	20.40	20.83	90.40	91.16
1.00	1.91	20.20	20.77	90.20	90.92

4.2 Preliminary Studies

As seen in Figure 4.3, it took around 3 minutes for the agar gel to reach the target temperature which is 42.5°C. After that time the system was able to keep the temperature constant by keeping the laser output power around 80-100%. For liver tissue, however,it took less than 10 seconds for lamb liver tissue to reach the target temperature. Due to the rapid changes in the temperature of the sample, the control parameters had to be corrected by changing the flowchart as mentioned in the methods section (Figure 3.2). After this correction, the system successfully kept the sample at a constant temperature by adjusting the laser output power between 20-100% of the maximum output power.

Figure 4.2 was generated using the temperature data collected after the samples reached the target temperature. Figure 4.2 revealed that the temperature-controlled laser system was able to keep the agar gel temperature slightly higher than the target temperature, with a median value of 42.7°C. The same figure reveals that the median temperature for the lamb liver tissue was calculated as 42.9°C. The 25% and 75% per-

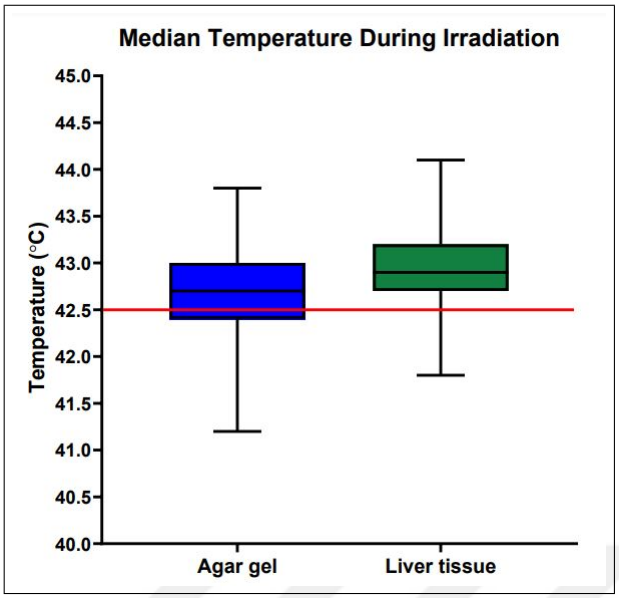


Figure 4.2 Box and whisker plot of the temperatures after the samples reach the target temperature, 42.5°C, as indicated by the dashed line.

centiles for agar gel were 42.5°C and 43.0°C, respectively. The 25% and 75% percentiles for lamb liver tissue were 42.7°C and 43.2°C, respectively.

4.3 Photothermal Applications

The first experiment was conducted to validate the algorithm, using agar gel as the target material. The software flow was monitored and validated during the experiment via the debug port of the MCU. The temperature increase rate of the target surface was detected and gCoefficient value was setted as 30.

As seen in Figure 4.4a, it took around 3 minutes for the agar gel to reach the target temperature which is 42.5°C. After that time the system was able to keep the temperature constant by keeping the laser output power around 80-100% as expected. Heat map of 32x32 pixel was acquired at an instant during agar gel irradiation as seen in Figure 4.4b.

The second, third and forth experiment was conducted using lamb liver tissue

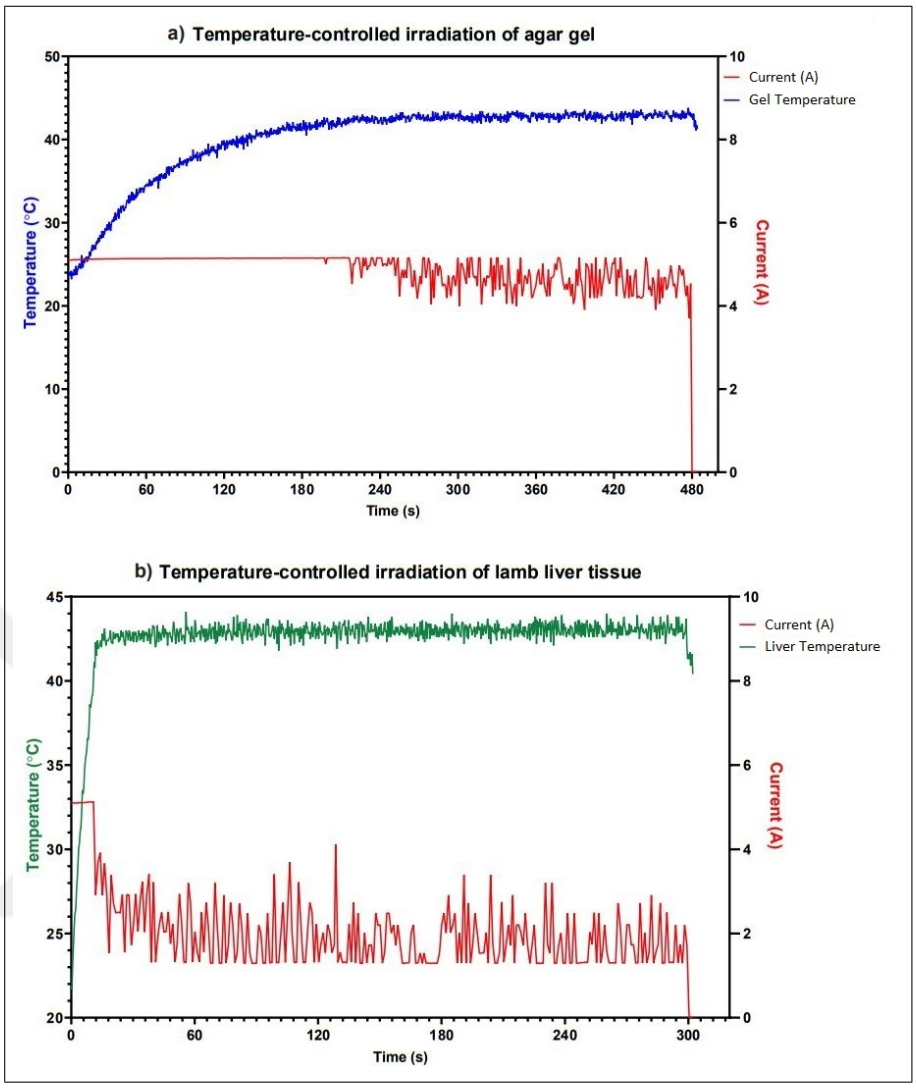


Figure 4.3 (a) Temperature of agar gel (left y-axis, indicated as blue) and laser current (right y-axis, indicated as red) during irradiation at a target temperature of 42.5°C.(b) Temperature of lamb liver tissue (left y-axis, indicated as green) and laser current (right y-axis, indicated as red) during irradiation at a target temperature of 42.5°C.

with target temperatures of 50°C, 60°C and 70°C respectively, employing the validated algorithm. The system was able detect the surface temperature increase rate for both lamb liver and agar gel experiments and set the gCoefficient value as 0 for lamb liver and 30 for agar gel. In other words the system can identify the surface thermal characteristics and set the optimum laser exposure algorithm accordingly.

It took nearly 19.5s to reach the target temperature of 50°C as seen in Figure 4.4c. After that time the system was able to keep the temperature constant by keeping the laser output power around 20-100% as expected. Heat map of 32x32 pixel was

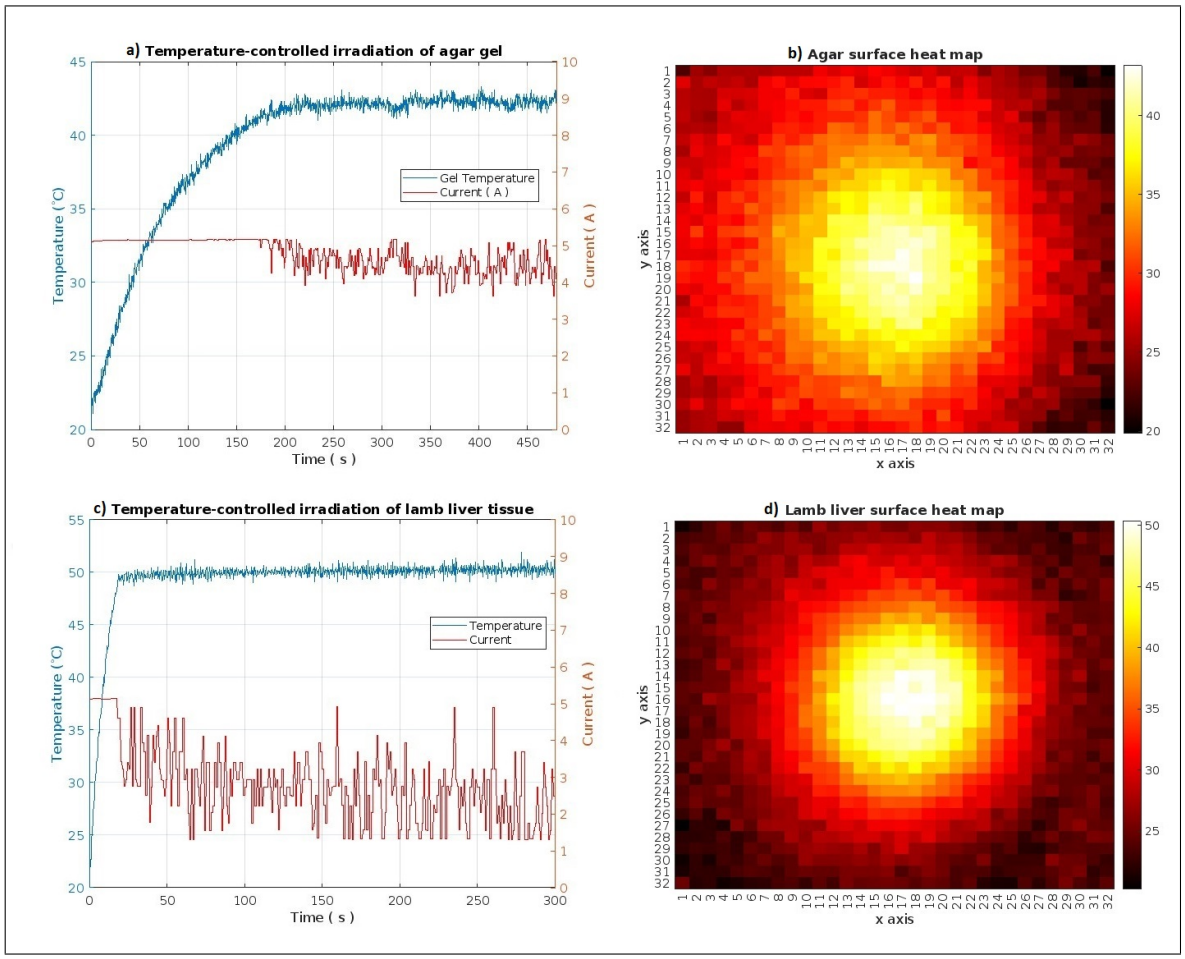


Figure 4.4 (a) Temperature of agar gel (left y-axis, indicated as blue) and laser current (right y-axis, indicated as red) during irradiation at a target temperature of 42.5°C. (b) A 32x32 heat map was acquired at an instant during agar gel irradiation at a target temperature of 42.5°C. (c) Temperature of lamb liver tissue (left y-axis, indicated as green) and laser current (right y-axis, indicated as red) during irradiation at a target temperature of 50°C. (d) A 32x32 heat map was acquired at an instant during the irradiation of lamb liver tissue at a target temperature of 50°C

acquired at an instant during agar gel irradiation as seen in Figure 4.4d.

It took nearly 59.5s to reach the target temperature of 60°C as seen in Figure 4.5a. After that time the system was able to keep the temperature constant by keeping the laser output power around 20-100% as expected. Heat map of 32x32 pixel was acquired at an instant during agar gel irradiation as seen in Figure 4.5b.

It took nearly 127.5s to reach the target temperature of 70°C as seen in Figure 4.5c. After that time the system was able to keep the temperature constant by keeping

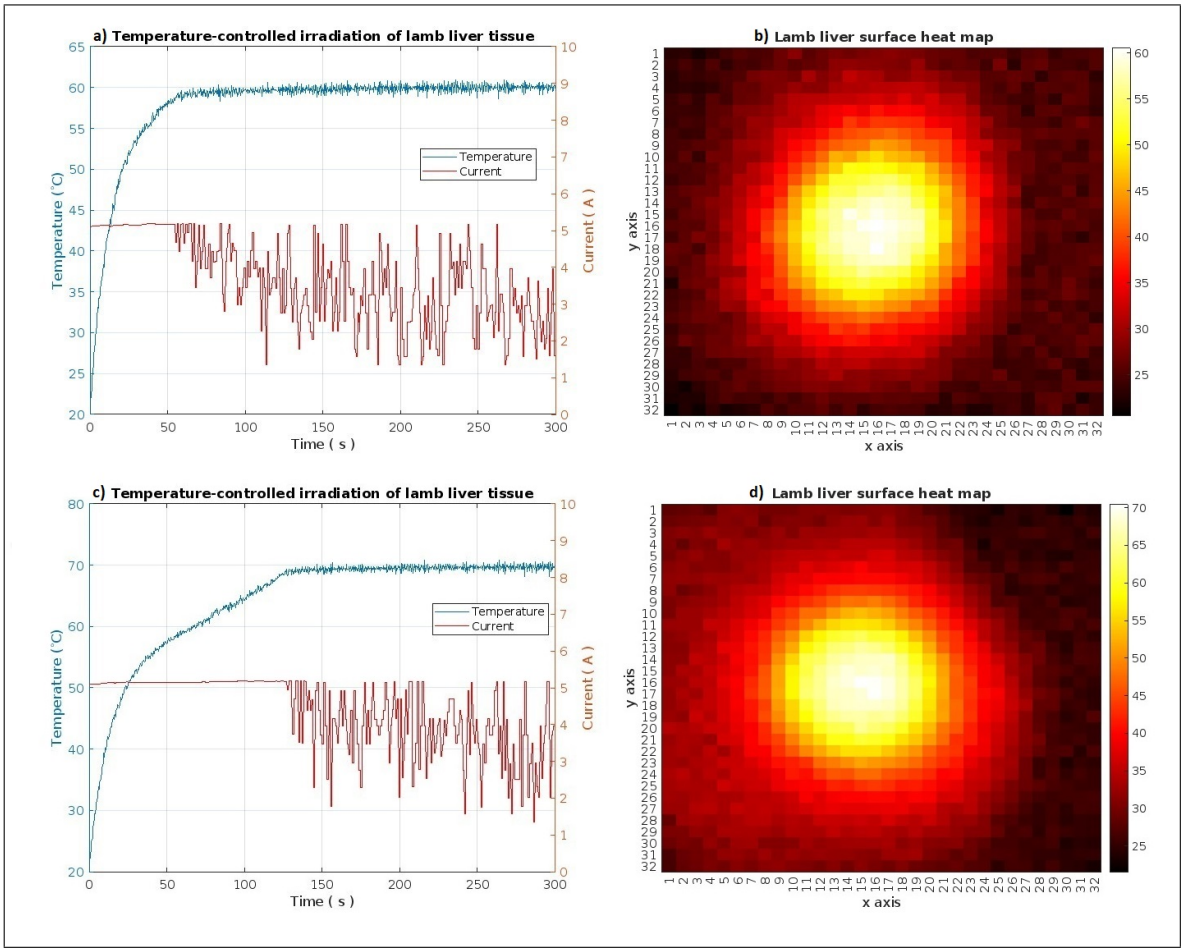


Figure 4.5 (a) Temperature of lamb liver tissue (left y-axis, indicated as blue) and laser current (right y-axis, indicated as red) during irradiation at a target temperature of 60°C. (b) A 32x32 heat map was acquired at an instant during the irradiation of lamb liver tissue at a target temperature of 60°C. (c) Temperature of lamb liver tissue (left y-axis, indicated as green) and laser current (right y-axis, indicated as red) during irradiation at a target temperature of 70°C. (d) A 32x32 heat map was acquired at an instant during the irradiation of lamb liver tissue at a target temperature of 70°C

the laser output power around 20-100% as expected. Heat map of 32x32 pixel was acquired at an instant during agar gel irradiation as seen in Figure 4.5d.

Figure 4.6 was generated as box and whiskers plot using the temperature data collected after the samples reached the target temperature. The red horizontal lines shows medians, the blue boxes indicate interquartile ranges and the red "+" signs are the outliers. Figure 4.6a revealed that the temperature-controlled laser system was able to keep the agar gel temperature slightly lower than the target temperature, with a median value of 42.1°C for first experiment and third, 42.2°C for second experiment.

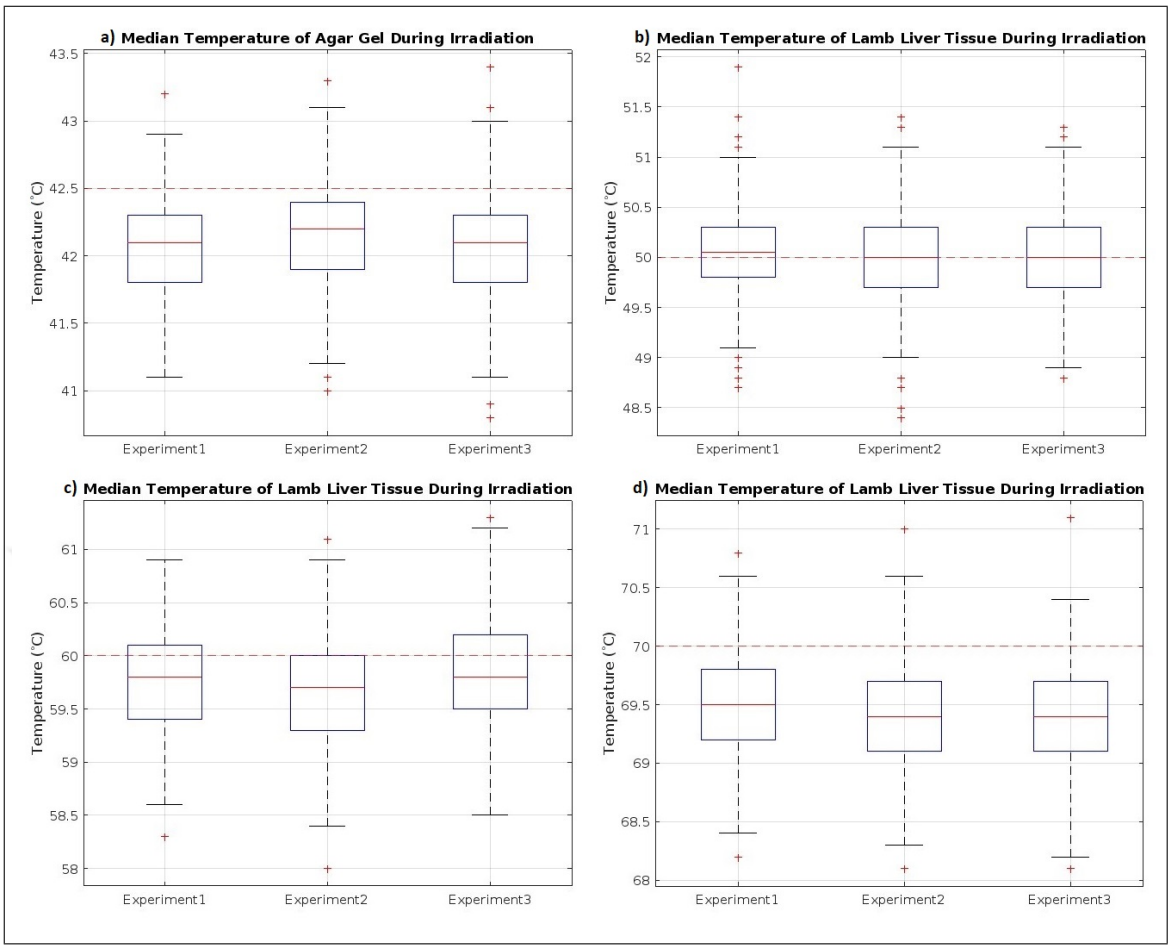


Figure 4.6 (a) Box and whisker plot of the temperatures agar gel reach the target temperature, 42.5°C, as indicated by the dashed line. (b) Box and whisker plot of the temperatures lamb liver reach the target temperature, 50°C, as indicated by the dashed line. (c) Box and whisker plot of the temperatures lamb liver reach the target temperature, 60°C, as indicated by the dashed line. (d) Box and whisker plot of the temperatures lamb liver reach the target temperature, 70°C, as indicated by the dashed line.

The Figure 4.6b reveals that the median temperatures for the lamb liver tissue were calculated as 50.05°C for first experiment, 50.0°C for second and the third experiment. Moreover in Figure 4.6c the median temperatures were calculated as 59.80°C for the first and third experiment, 59.7°C for second experiment and in Figure 4.6d the median temperatures were calculated as 69.5°C for the first experiment and 69.4°C for the second and the third experiment.

The 25% and 75% percentiles for agar gel were 41.8°C and 42.3°C for the first experiment, 41.9°C and 42.2°C for the second experiment, 41.8°C and 42.3°C for the

Table 4.2
The 25% and 75% percentiles for lamb liver tissues according to Figure 4.6b, Figure 4.6c and Figure 4.6d.

Experiments	50°C 75% pctl	60°C 75% pctl	70°C 75% pctl
Experiment1	50.30	60.10	69.80
Experiment2	50.30	60.00	69.70
Experiment3	50.30	60.20	69.70

Experiments	50°C 25% pctl	60°C 25% pctl	70°C 25% pctl
Experiment1	49.80	59.40	69.20
Experiment2	49.70	59.30	69.10
Experiment3	49.70	59.50	69.10

third experiment, respectively. The 25% and 75% percentiles for lamb liver tissues are listed in the Table 4.2. According to the results, the system was able to maintain the temperature at the preset value for both the agar gel and lamb liver tissue.

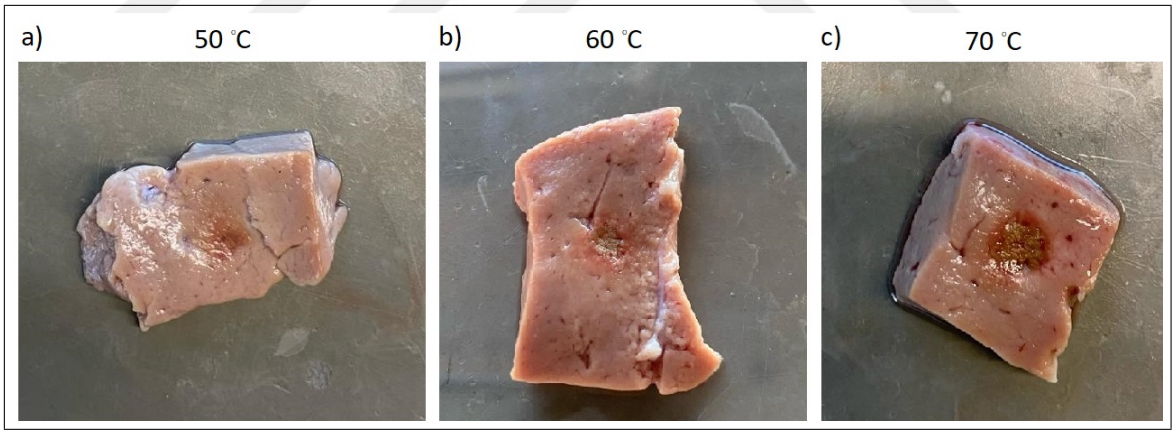


Figure 4.7 (a) Lamb liver tissue irradiated at 50°C (b)Lamb liver tissue irradiated at 60°C (c)Lamb liver tissue irradiated at 70°C

In Figure 4.7 photothermal effects of temperature-controlled laser system on lamb liver tissues is shown. Laser-induced hyperthermia and coagulation can be distinguished visually between the Figures 4.6a, Figures 4.6b and Figures 4.6c. We can say that the expected thermal damage is only seen on the irradiated surfaces, not on the surrounding tissues.

4.4 Constant Power Irradiation of Lamb Liver Tissue

Constant power laser irradiation was applied on lamb liver tissues to compare the results between temperature-controlled and constant power. When the current versus time data from Figure 4.3b, Figure 4.4c, Figure 4.5a and Figure 4.5c was processed using the "trapz(x,y)" command in MATLAB, the resulting value indicated a laser output power of 1.24W, 1.51W, 2.00W and 2.57W respectively, which was applied for 300s. This experiments were repeated three times, and the results shown in Figure 4.8.

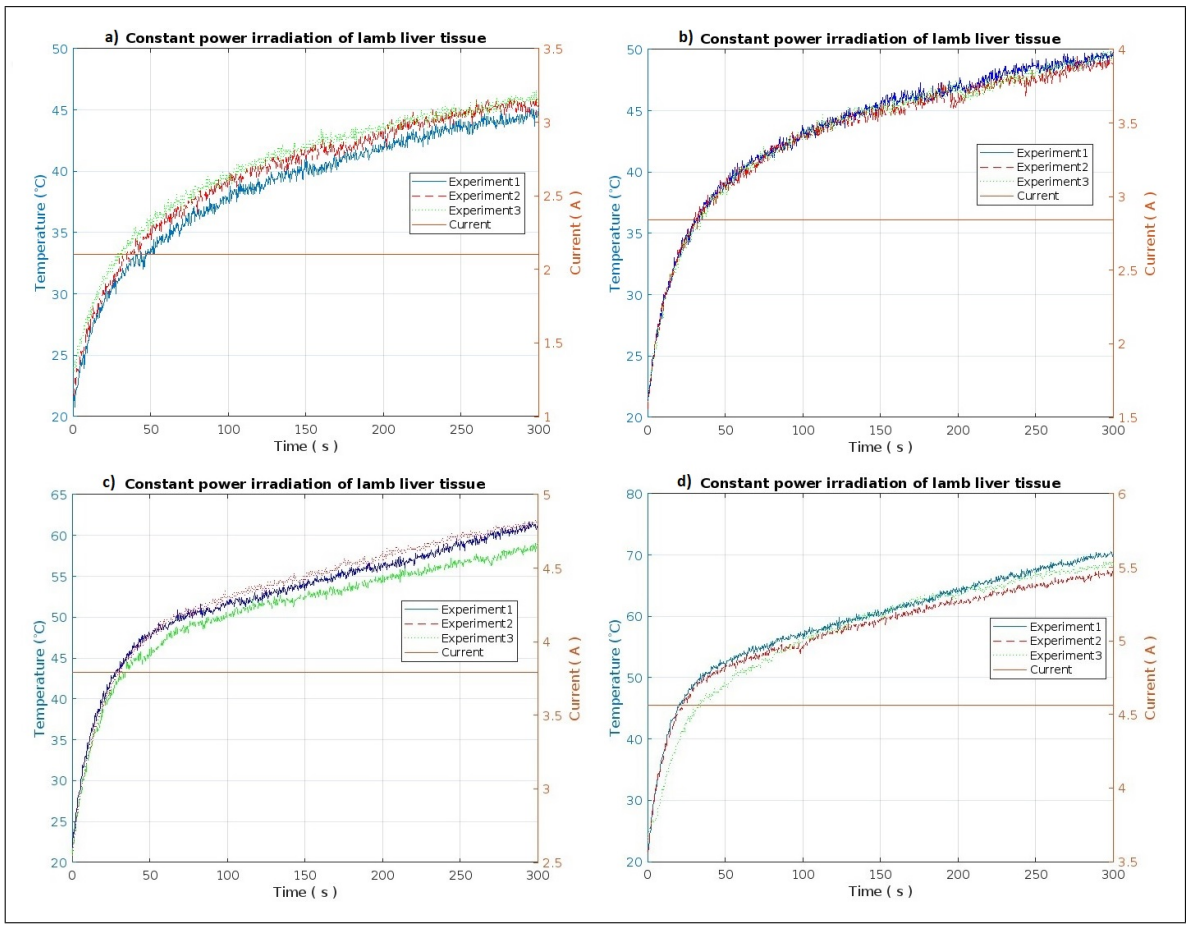


Figure 4.8 (a) Constant power irradiation of lamb liver tissue for 42.5°C. (b) Constant power irradiation of lamb liver tissue for 50°C (c) Constant power irradiation of lamb liver tissue for 60°C (d) Constant power irradiation of lamb liver tissue for 70°C

Temperature-controlled laser system was able to keep the surface temperature at a median value of 42.9°C which is slightly above the target value of 42.5°C as seen in Figure 4.3b. On the other hand, during constant power irradiation, the target tem-

perature was achieved by 150s and reached above 45°C at the end of the experiment as seen in Figure 4.8a. Meanwhile in the temperature-controlled experiment the targeted value was reached at approximately 10s and kept till the end of the experiment as seen in Figure 4.3b.

In the 50°C experiment, temperature-controlled laser system was able to keep the surface temperature at a median value of 50.05°C as seen in Figure 4.4c. On the other hand, during constant power irradiation, 45°C reached at 140s and 50°C of target temperature being reached at the end of the experiment.

In the 60°C experiment, the temperature-controlled laser system was able to maintain the surface temperature at a median value of 59.80°C, as seen in Figure 4.5a. On the other hand, during constant power irradiation, the surface temperature reached 50°C at 96 seconds and the target temperature of 60°C was achieved by the end of the experiment in only two samples. In Experiment 3, the surface temperature only reached at 59.10°C.

In the 70°C experiment, temperature-controlled laser system was able to keep the surface temperature at a median value of 69.50°C as seen in Figure 4.5c. On the other hand, during constant power irradiation, 60°C reached at 141s and 70°C of target temperature reached at the end of the experiment only in one sample. In Experiment 2 and 3, the surface temperature only reached at 67.40°C and 69.00°C, respectively.

5. DISCUSSION

Photothermal treatments require precise control of the tissue temperature. The current study aimed to develop an IR array-based temperature-controlled laser system that could potentially be used safely and effectively in clinics. The results of the first experiment given in Figure 4.1 showed that the measurements of the purchased IR array sensor were comparable with respect to a commercial handheld IR thermometer.

The temperature-controlled laser system was then used to irradiate agar gels and liver tissues in preliminary studies. The temperature of both samples could be increased up to 42.5°C and kept at this temperature for around 5 minutes. However, as shown in Figure 4.3, the rate of temperature increase was very low compared to the liver tissue. The difference in temperature increase rate is primarily associated with the difference in absorption of 808 nm light by the samples. Since liver tissue is nontransparent and highly turbid, it is expected that the light is scattered and eventually absorbed. Conversely, the transparent agar gel transmitted most of the light and absorbed a smaller portion. These results emphasized the importance of selecting the correct experimental model, as well as the urge to correct the system based on the absorption properties of the samples. Therefore, some of the commands stated in the flowcharts were corrected for liver tissue as shown in Figure 3.2b. In that case, the system could successfully keep the temperature at the target value. As shown in Figure 4.2, there was a slight difference between the median temperatures and the target temperature, which can be overcome by optimizing the settings of the system.

The temperature increase rate detection algorithm, developed as shown in Figure 3.5a based on the results of preliminary studies, was integrated into the laser irradiation control function. The agar gel experiment was conducted to validate the algorithm. The temperature of agar gel sample reach up to 42.2°C and and kept at this temperature for around 5 minutes. In addition, lamb liver tissue experiments conducted for the temperatures 50°C, 60°C and 70°C by employing the same algorithm.

The system was able to identify the surface thermal characteristics and set the optimum laser exposure algorithm accordingly. Figure 4.6 reveals that the median value was the closest to the target value in the "50°C experiment". The median temperature in the "60°C and 70°C experiments" were slightly lower than the target temperature. As the target temperature increases, the deviation increases accordingly. Currently, the minimum laser output is set to a static value of 20%, as shown in Figure 3.5b. Introducing an update that determines the minimum laser output based on the target temperature, thereby making it a dynamic variable, would optimize the results.

Lamb liver tissues were irradiated with constant power at four different temperatures: 42.5°C, 50°C, 60°C, and 70°C. For each temperature, the experiments repeated for three times using pre-calculated dosimeter settings. Regardless of the applied dosimeter, the graph curves of each experiment displayed a similar formation, with a noticeable deviation from the target temperature as seen in Figure 4.8. On the other hand, in the temperature-controlled experiments, the target temperature was reached with a slight variance. Even though the same laser power was applied to the liver tissues for the same time of period, the results clearly differed from each other including the duration of target temperature.

The system is currently a promising prototype which fulfilled the expectations with negligible deviation. The c-mount laser diode used in the system can be easily replaced, enabling the adoption of different wavelengths with minimal adjustment. The precision of the system can be improved by updating the software. Our future objective is to achieve a more compact design to use the system in further animal studies and clinical trials.

APPENDIX A. SCHEMATICS OF ELECTRONIC CONTROL UNIT

This section presents the schematics design of electronic control unit, as seen in Figure A.1, Figure A.2 and Figure A.3 and was drawn in Cadsoft EAGLE.

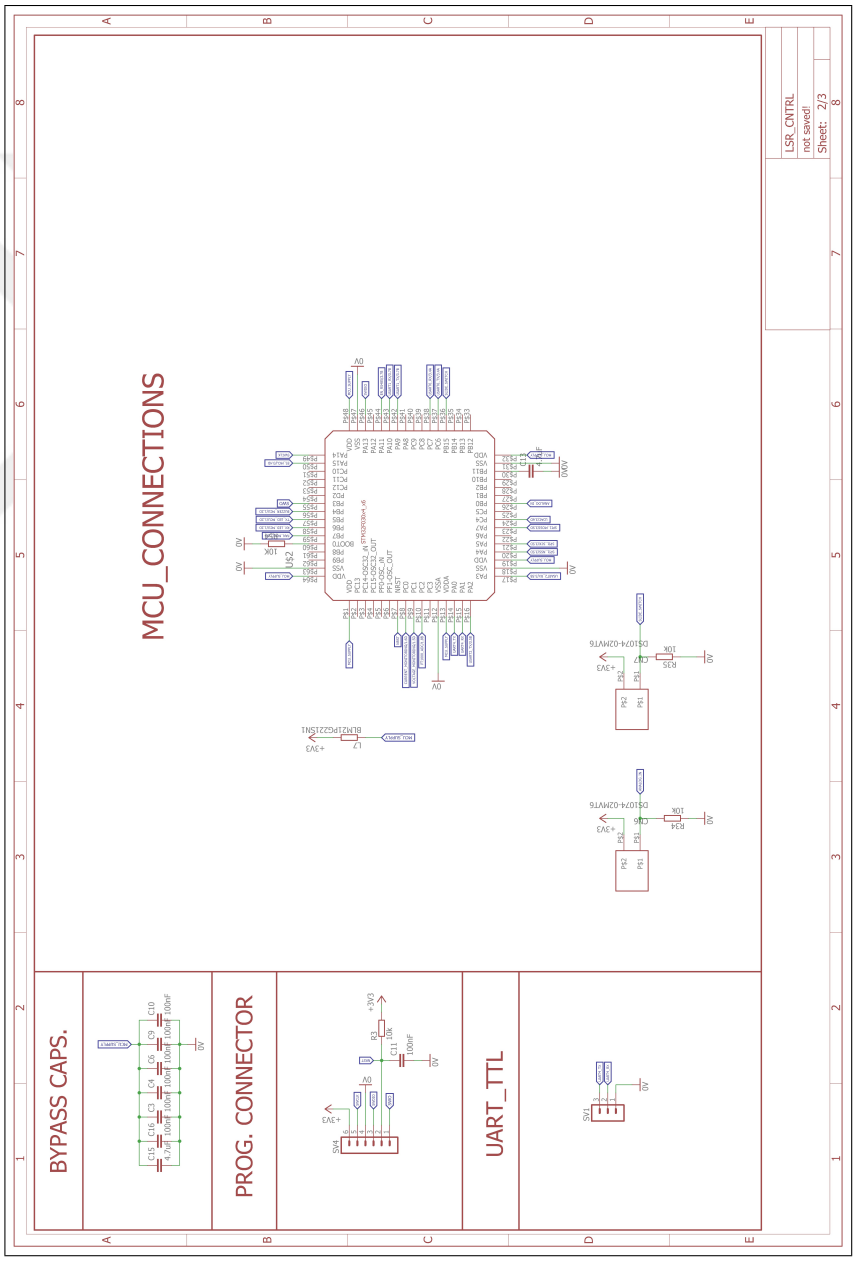


Figure A.1 Schematics design of electronic control unit sheet1.

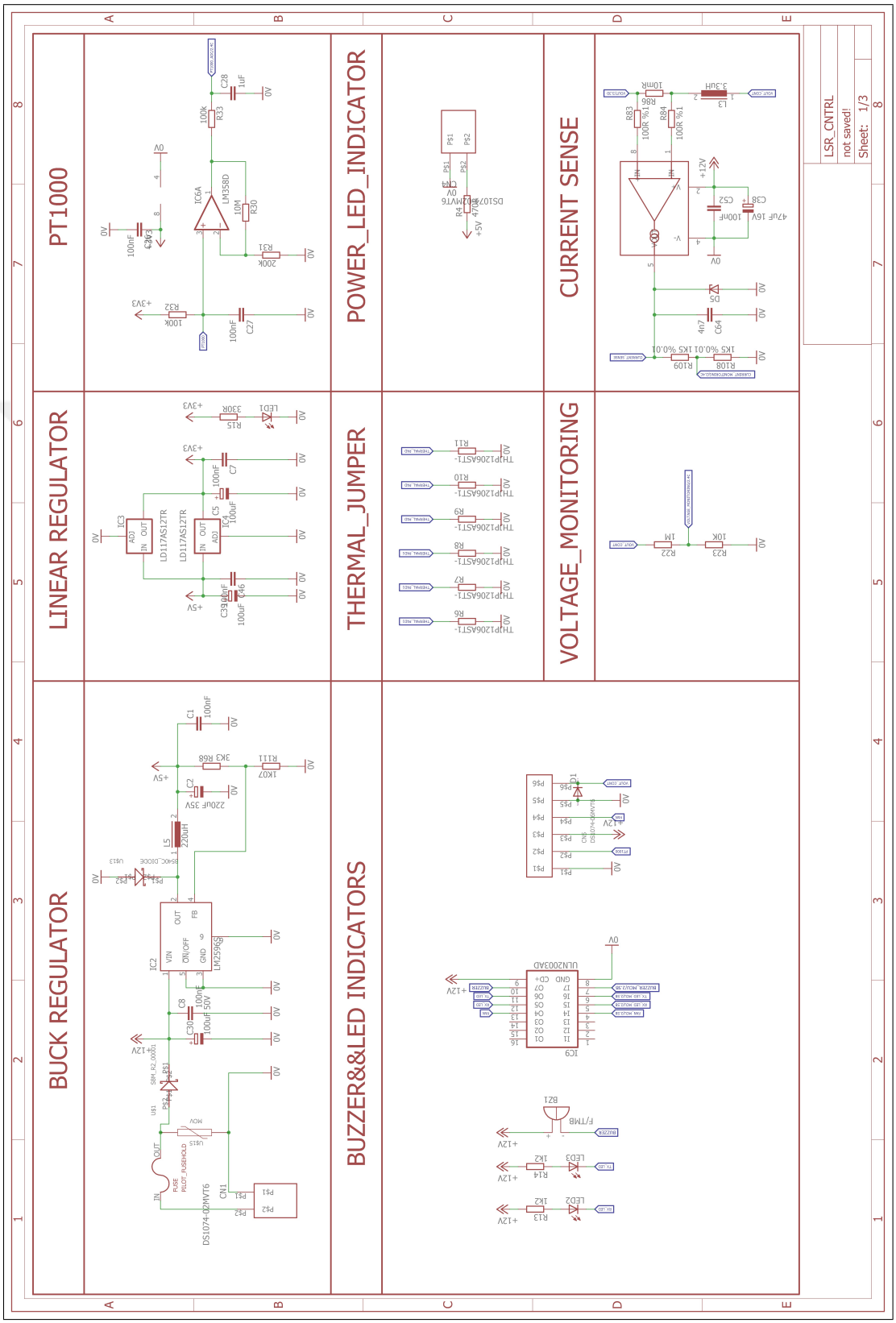


Figure A.2 Schematics design of electronic control unit sheet2.

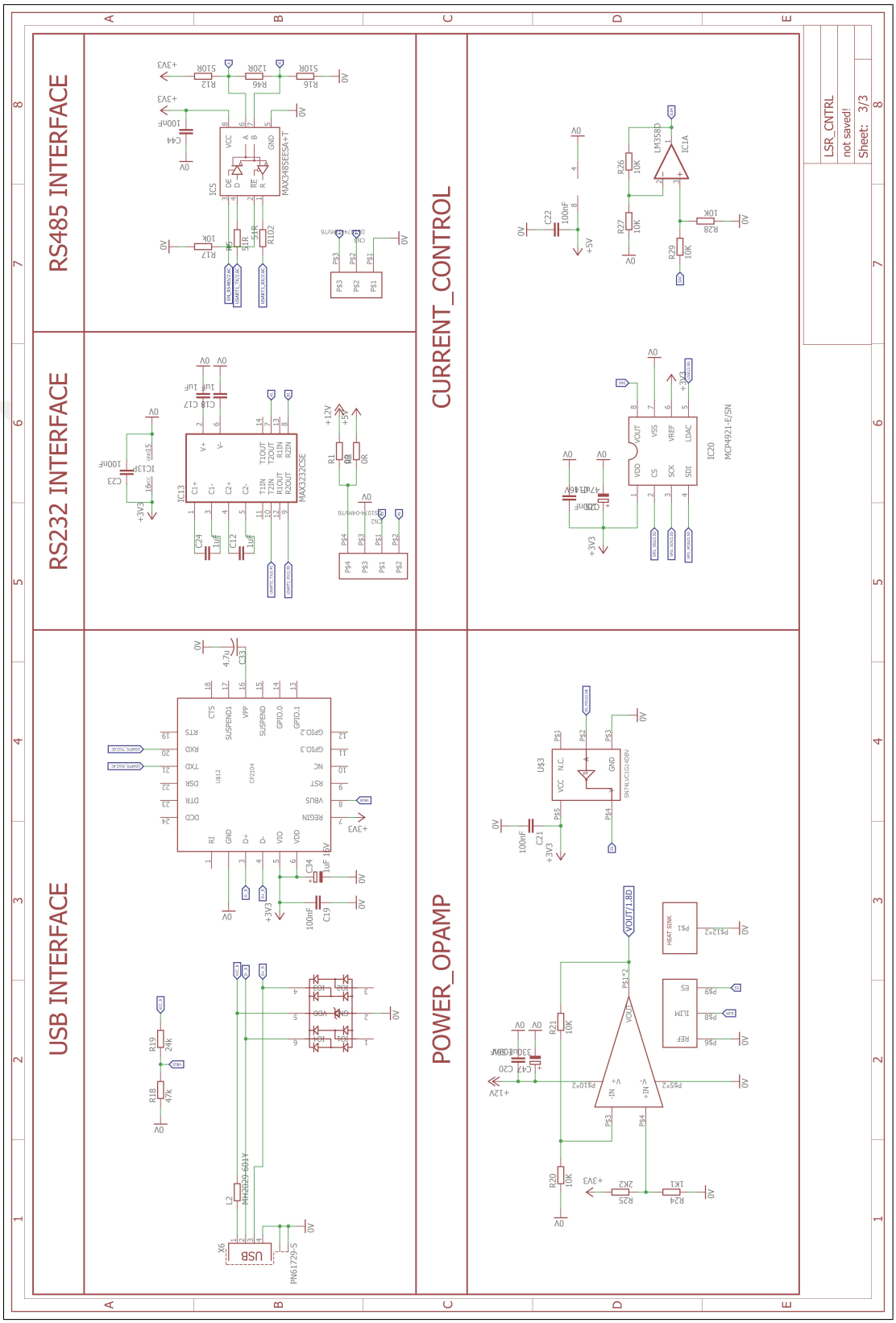


Figure A.3 Schematics design of electronic control unit sheet3.

APPENDIX B. PCB DESIGN OF ELECTRONIC CONTROL UNIT

This section presents the printed circuit board design of the electronic control unit, as seen in Figure B.1 and was drawn using Cadsoft EAGLE.

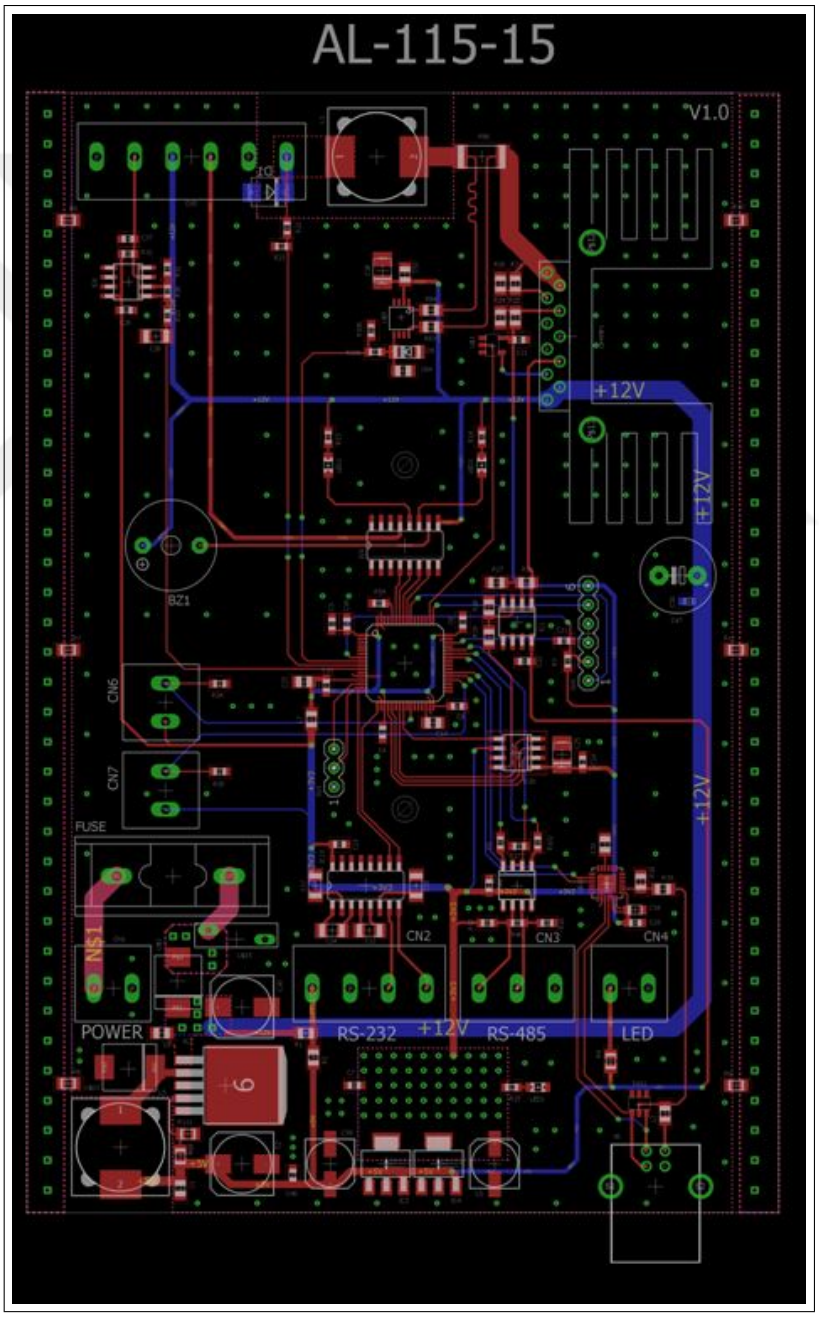


Figure B.1 PCB design of ECU.

APPENDIX C. SCHEMATICS OF IR ARRAY UNIT

This section presents the schematics design of IR array unit, as seen in Figure C.1 and Figure C.2 and was drawn in Cadsoft EAGLE.

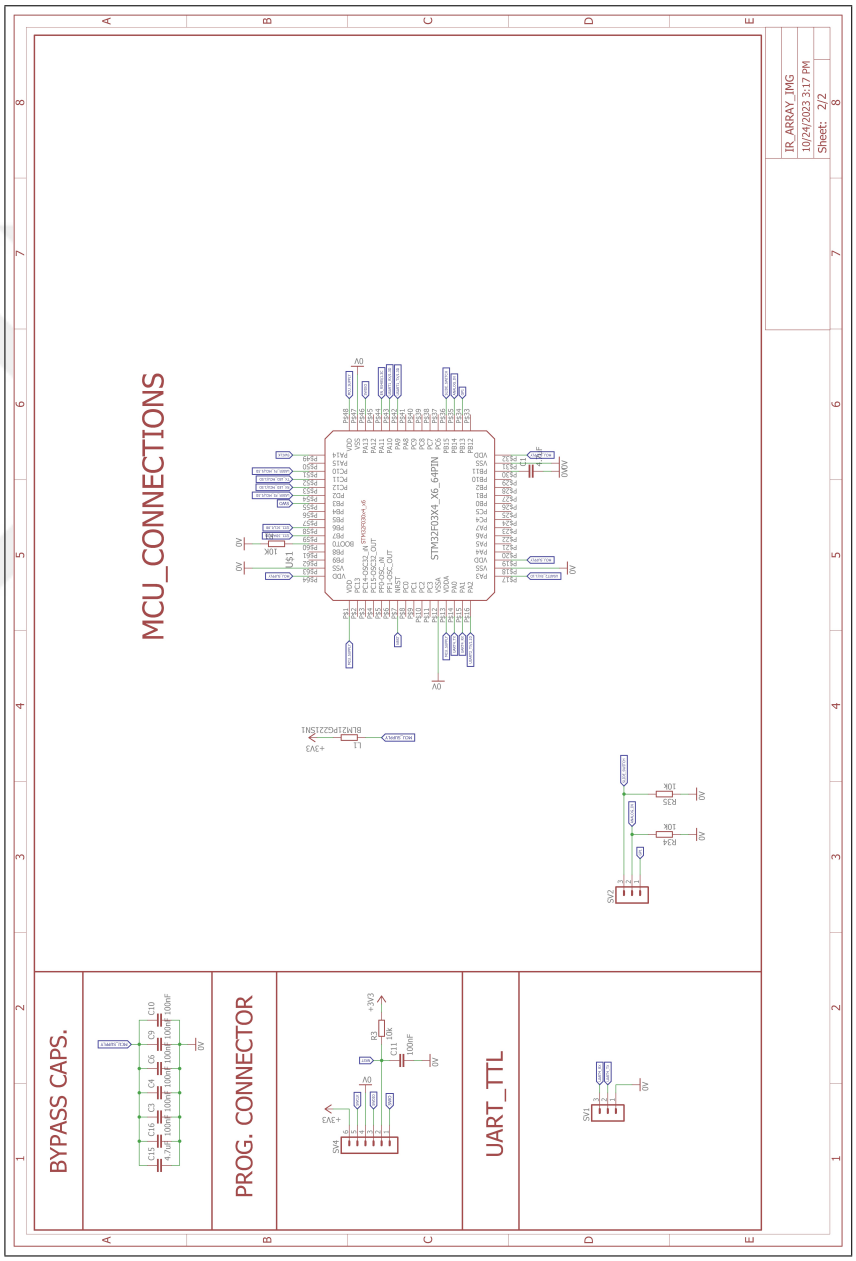


Figure C.1 Schematics design of IR array unit sheet1.

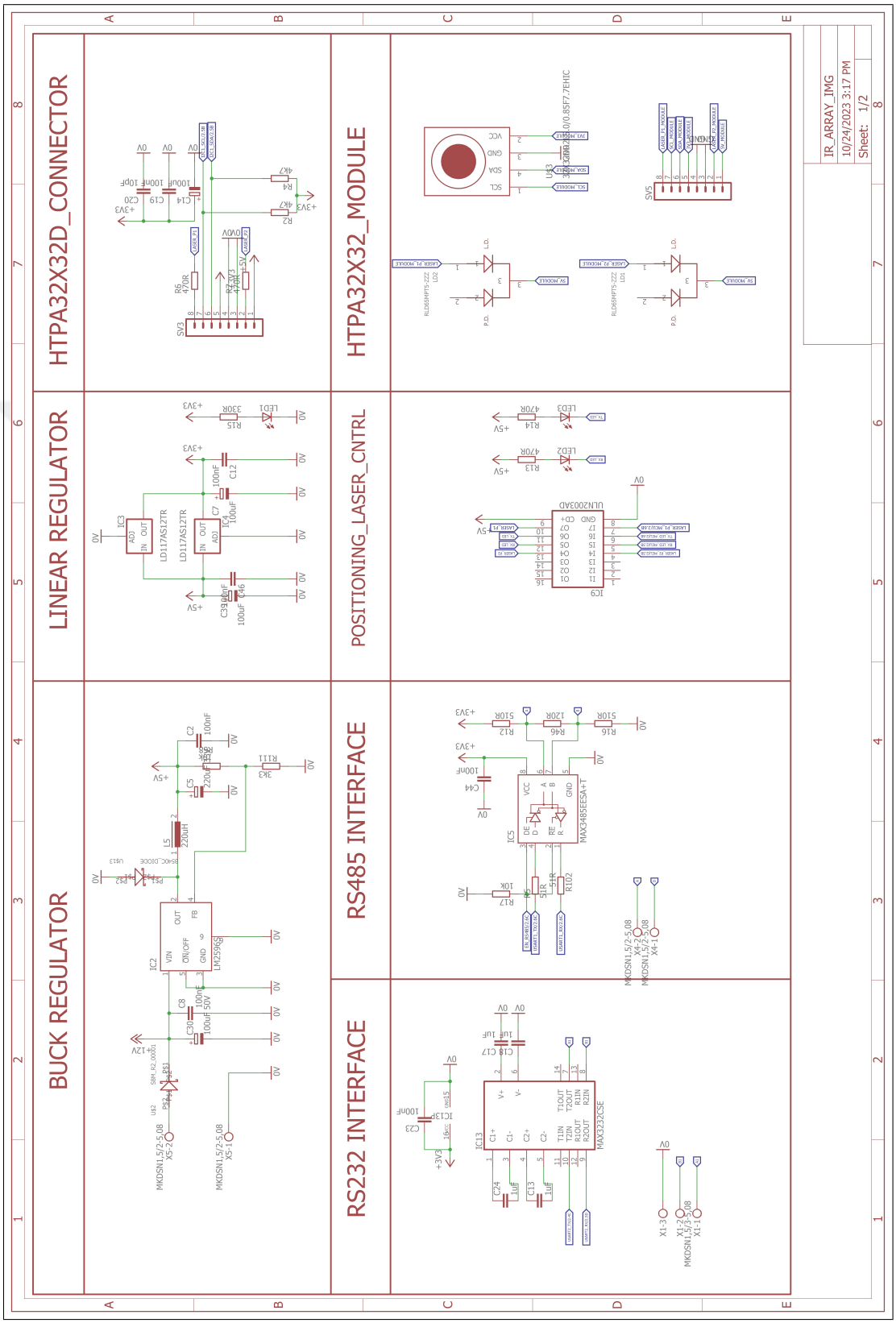


Figure C.2 Schematics design of IR array unit sheet2.

APPENDIX D. PCB DESIGN OF IR ARRAY UNIT

This section presents the printed circuit board design of the IR array unit, as seen in Figure D.1 and was drawn using Cadsoft EAGLE.

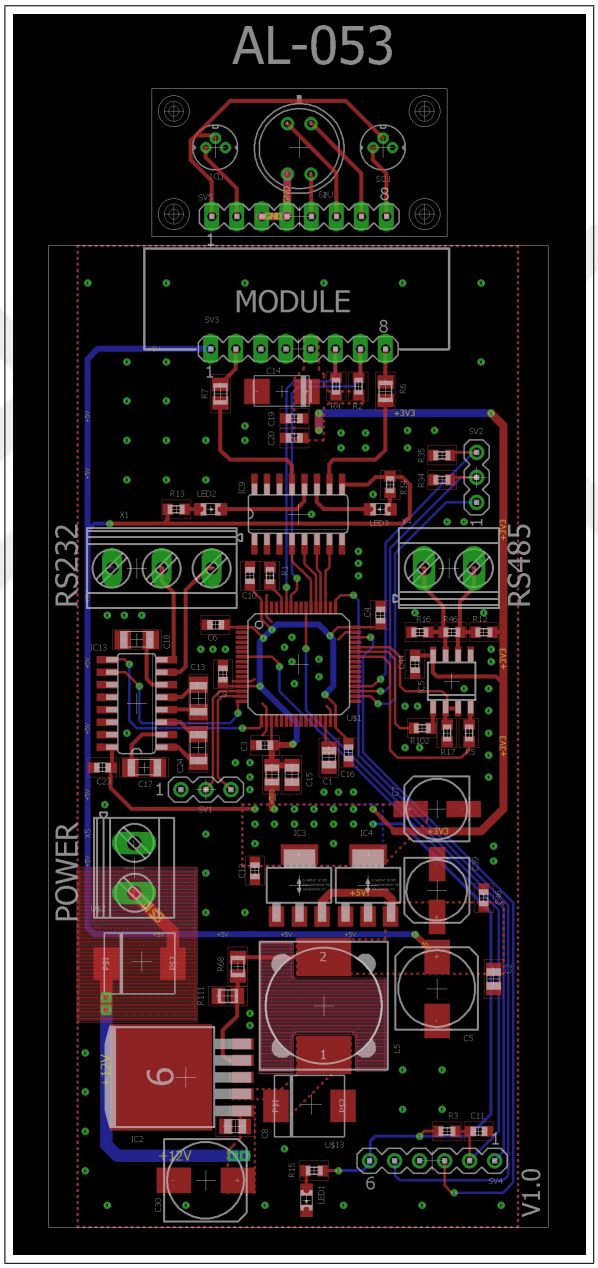


Figure D.1 PCB design of IR array unit.

REFERENCES

1. Townes, C. H., "How the Laser Happened: Adventures of a Scientist," *Oxford University Press*, 1999.

2. Neimz, M., "Laser tissue interactions fundamentals and applications," *Heidelberg: Springer*, 2003.

3. Jacques, S. L., "Laser-tissue interactions. Photochemical, photothermal, and photomechanical," *Surg Clin North Am*, Vol. 72, pp. 531–58, Jun 1992.

4. J. Wang, N. S., and H. Shen, "Successful Treatment of Multiple Plantar and Periungual Warts by Local Hyperthermia Treatment: A Case Report," *Clin Cosmet Investig Dermatol*, Vol. 16, pp. 981–985, 2023.

5. Huo, W., and et al., "Local Hyperthermia Versus Cryotherapy for Treatment of Plantar Warts: A Prospective Multi-centre Non-randomized Concurrent Controlled Clinical Trial," *Acta Derm Venereol*, Vol. 102, Feb 28 2022.

6. X. Chen, Y. Xu, L. H., and A. Chen, "Clinical observation and study of local hyperthermia for treating plantar warts: A pilot study with 38 patients," *Front Med (Lausanne)*, Vol. 10, 2023.

7. H. F. Wang, R. Z. An, L. M., and X. H. Gao, "Recurrent condyloma acuminatum after cryotherapy plus photodynamic therapy successfully treated by local hyperthermia: A case report," *Dermatol Ther*, Vol. 35, pp. 981–985, Oct 2022.

8. J. Hahl, R. Haapiainen, J. O. P. P., and T. Schroder, "Laser-induced hyperthermia in the treatment of liver tumors," *Lasers Surg Med*, Vol. 10, pp. 319–21, 1990.

9. A. C. Steger, W. R. Lees, K. W., and S. G. Bown, "Interstitial laser hyperthermia: a new approach to local destruction of tumours," *Lasers Surg Med*, Vol. 299, pp. 362–5, Aug 5 1989.

10. Thomsen, S., and J. A. Pearce, "Thermal Damage and Rate Processes in Biologic Tissues," *Optical Thermal Response of Laser-Irradiated Tissue, Second Edition*, pp. 487–549, 2011.

11. Jacques, S. L., "Interstitial laser hyperthermia: a new approach to local destruction of tumours," *Phys Med Biol*, Vol. 58, pp. R37–61, Jun 7 2013.

12. Ö. D. Kaya, İ.; Çilesiz, İ. G. M., "Controlling Laser Irradiation with Tissue Temperature Feedback Enhances Photothermal Applications: Ex-Vivo Evaluation on Bovine Liver," *Applied Sciences*, Vol. 13, 2023.

13. Simhon, D., and et al., "Temperature-controlled laser-soldering system and its clinical application for bonding skin incisions," *J Biomed Opt*, Vol. 20, 2015.

14. Schlott, K., and et al., "Automatic temperature controlled retinal photocoagulation," *J Biomed Opt*, Vol. 17, Jun 2012.

15. Poppas, D. P., and et al., "Temperature-controlled laser photocoagulation of soft tissue: in vivo evaluation using a tissue welding model," *Lasers Surg Med*, Vol. 18, pp. 335–44, 1996.

16. Shinsuke Nomura, M. A., and et al., "Thermal Sensor Circuit Using Thermography for Temperature-Controlled Laser Hyperthermia," *Journal of Sensors*, Vol. 2017, 9 October 2017.

17. EDR-120-12, D. D., "https://www.meanwell.com/Upload/PDF/EDR-120/EDR-120-SPEC.PDF," *Meanwell*.

18. Products, B.-B., "https://www.ti.com/lit/ds/symlink/opa549.pdf," *Burr-Brown Products from Texas Instruments*, Last Rev. October 2005.

19. Technology, L., "https://www.analog.com/media/en/technical-documentation/data-sheets/6105fa.pdf," *Linear Technology Corporation from Analog Devices*.

20. Microchip, "https://ww1.microchip.com/downloads/en/DeviceDoc/21897B.pdf," *Microchip Technology Incorporated*, Last Rev. February 2007.

21. Instruments, T., "https://www.ti.com/lit/ds/symlink/lm2596.pdf," *Texas Instruments*, Last Rev. March 2023.

22. Microelectronics, S., "https://www.st.com/resource/en/datasheet/stm32f446re.pdf," *ST Microelectronics*, Last Rev. January 2021.

23. Instruments, T., "https://www.ti.com/sitesearch/en-us/docs/universalsearch.tsp?langPref=en-USq=max3232idrf-technicalDocuments," *Texas Instruments*, Last Rev. June 2021.

24. Devices, A., "https://www.analog.com/media/cn/technical-documentation/data-sheets/2023.pdf," *Analog Devices*, Rev 1; 5/19.

25. Labs, S., "https://www.silabs.com/documents/public/data-sheets/cp2104.pdf," *Silicon Labs*, Last Rev. January 20, 2017.

26. Manabu Harada, Y. M., and et al., "Temperature-controlled laser thermal therapy system using a newly developed laparoscopic system equipped with an ultra-compact thermographic camera," *Scientific Reports*, Vol. 12, 2022/10/31.

27. Sensor, H., "https://www.heimannsensor.com/32x32," *HEIMANN Sensor GmbH*.

28. Instruments, T., "https://www.ti.com/lit/ds/symlink/uln2003a.pdf," *Texas Instruments*, Last Rev. February 2024.